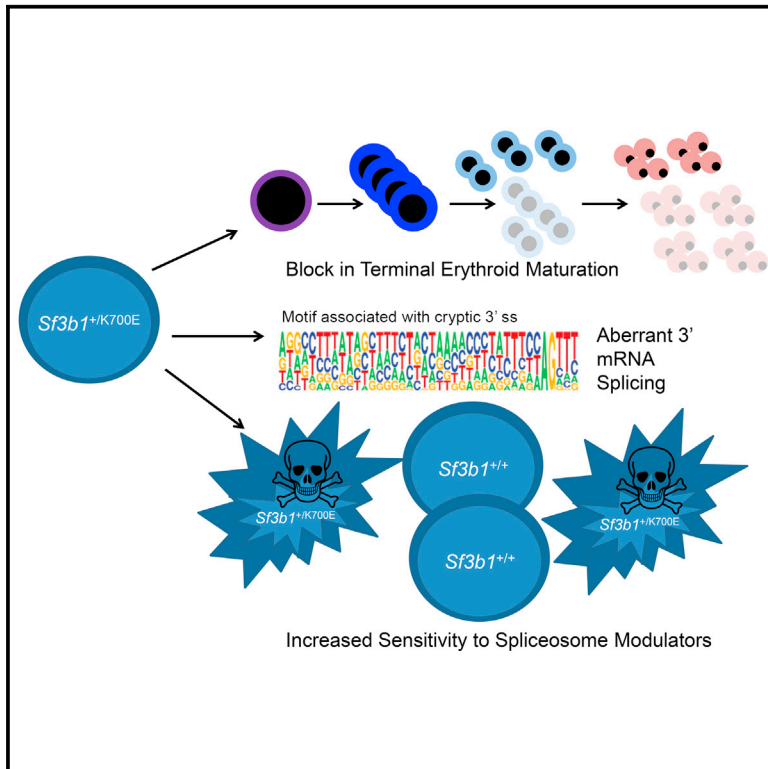


# Cancer Cell

## Physiologic Expression of *Sf3b1*<sup>K700E</sup> Causes Impaired Erythropoiesis, Aberrant Splicing, and Sensitivity to Therapeutic Spliceosome Modulation

### Graphical Abstract



### Authors

Esther A. Obeng, Ryan J. Chappell, Michael Seiler, ..., Catherine J. Wu, Mark D. Fleming, Benjamin L. Ebert

### Correspondence

bebert@partners.org

### In Brief

Obeng et al. generate knockin mice with *Sf3b1*<sup>K700E</sup>, a prevalent mutation in myelodysplastic syndrome (MDS). *Sf3b1*<sup>+/K700E</sup> mice display characteristics of MDS. Mouse and human MDS cells expressing SF3B1<sup>K700E</sup> exhibit aberrant 3' splice-site selection, and SF3B1<sup>K700E</sup> sensitizes cells to a spliceosome modulator.

### Highlights

- *Sf3b1*<sup>+/K700E</sup> mice develop a progressive macrocytic anemia and myelodysplasia
- Mutant SF3B1 causes aberrant 3' splice-site selection
- *Sf3b1*<sup>+/K700E</sup> and *Tet2* loss cause an earlier onset of MDS characteristics
- Spliceosome modulators selectively kill cells expressing SF3B1<sup>K700E</sup>

### Accession Numbers

GSE85712



# Physiologic Expression of *Sf3b1*<sup>K700E</sup> Causes Impaired Erythropoiesis, Aberrant Splicing, and Sensitivity to Therapeutic Spliceosome Modulation

Esther A. Obeng,<sup>1,2,3</sup> Ryan J. Chappell,<sup>3</sup> Michael Seiler,<sup>4</sup> Michelle C. Chen,<sup>3</sup> Dean R. Campagna,<sup>5</sup> Paul J. Schmidt,<sup>5</sup> Rebekka K. Schneider,<sup>3</sup> Allegra M. Lord,<sup>3</sup> Lili Wang,<sup>6</sup> Rutendo G. Gambe,<sup>6</sup> Marie E. McConkey,<sup>3</sup> Abdullah M. Ali,<sup>7</sup> Azra Raza,<sup>7</sup> Lihua Yu,<sup>4</sup> Silvia Buonamici,<sup>4</sup> Peter G. Smith,<sup>4</sup> Ann Mullally,<sup>3,8</sup> Catherine J. Wu,<sup>6,8</sup> Mark D. Fleming,<sup>5</sup> and Benjamin L. Ebert<sup>3,8,9,\*</sup>

<sup>1</sup>Department of Pediatric Oncology, Dana-Farber Cancer Institute, Boston, MA 02115, USA

<sup>2</sup>Division of Hematology/Oncology, Department of Medicine, Boston Children's Hospital, Boston, MA 02115, USA

<sup>3</sup>Division of Hematology, Department of Medicine, Brigham and Women's Hospital, Harvard Medical School, Boston, MA 02115, USA

<sup>4</sup>H3 Biomedicine, Inc., Cambridge, MA 03129, USA

<sup>5</sup>Department of Pathology, Boston Children's Hospital, Boston, MA 02115, USA

<sup>6</sup>Department of Medical Oncology, Dana-Farber Cancer Institute, Harvard Medical School, Boston, MA 02115, USA

<sup>7</sup>Division of Hematology/Oncology, Columbia University Medical Center, New York, NY 10027, USA

<sup>8</sup>Broad Institute of MIT and Harvard, Cambridge, MA 02142, USA

<sup>9</sup>Lead Contact

\*Correspondence: [bebert@partners.org](mailto:bebert@partners.org)

<http://dx.doi.org/10.1016/j.ccell.2016.08.006>

## SUMMARY

More than 80% of patients with the refractory anemia with ring sideroblasts subtype of myelodysplastic syndrome (MDS) have mutations in Splicing Factor 3B, Subunit 1 (*SF3B1*). We generated a conditional knockin mouse model of the most common *SF3B1* mutation, *Sf3b1*<sup>K700E</sup>. *Sf3b1*<sup>K700E</sup> mice develop macrocytic anemia due to a terminal erythroid maturation defect, erythroid dysplasia, and long-term hematopoietic stem cell (LT-HSC) expansion. *Sf3b1*<sup>K700E</sup> myeloid progenitors and *SF3B1*-mutant MDS patient samples demonstrate aberrant 3' splice-site selection associated with increased nonsense-mediated decay. *Tet2* loss cooperates with *Sf3b1*<sup>K700E</sup> to cause a more severe erythroid and LT-HSC phenotype. Furthermore, the spliceosome modulator, E7017, selectively kills *SF3B1*<sup>K700E</sup>-expressing cells. Thus, *SF3B1*<sup>K700E</sup> expression reflects the phenotype of the mutation in MDS and may be a therapeutic target in MDS.

## INTRODUCTION

Recurrent point mutations in components of the 3' mRNA splicing machinery are the most common mutations in patients with myelodysplastic syndromes (MDS) (Papaemmanuil et al., 2011; Visconte et al., 2012a; Welch et al., 2012; Yoshida et al., 2011). MDS is characterized by clonal hematopoiesis, peripheral

blood cytopenias, and a variable risk of transformation to acute myeloid leukemia. Splicing factor gene mutations in MDS are typically heterozygous, missense, and mutually exclusive of one another. The three most commonly mutated splicing factors in MDS, *SF3B1*, *U2AF1*, and *SRSF2*, are all involved in the initial steps of spliceosome assembly (Kramer, 1996; Will and Luhrmann, 2011; Yoshida et al., 2011).

## Significance

Somatic point mutations in components of the pre-mRNA spliceosome are the most common mutations in myelodysplastic syndromes (MDS). Here we demonstrate that mutation of the most commonly mutated splicing factor in MDS, *Sf3b1*, causes impaired red blood cell differentiation leading to anemia, an increase in long-term hematopoietic stem cells in the bone marrow, and myelodysplasia. We also show that mutant *SF3B1* causes increased aberrant 3' splice-site selection leading to increased nonsense-mediated decay. *Sf3b1* mutations cooperate with *Tet2* loss to cause an accelerated MDS phenotype. Cells expressing mutant *SF3B1* have increased sensitivity to the spliceosome modulator, E7107. These data show how mutant *SF3B1* affects hematopoiesis and mRNA splicing and identify spliceosome inhibitors as a potential new therapy for MDS.

The spliceosome is a large macromolecular complex composed of five small nuclear ribonucleoproteins (snRNPs) and more than 200 additional proteins (Chen and Manley, 2009). More than 90% of human genes undergo alternative splicing of precursor mRNA (pre-mRNA), a tightly regulated process that dramatically increases the complexity of the protein repertoire encoded by the genome (Becerra et al., 2015). The 5' splice site (ss) of an intron is typically defined by a GU dinucleotide. Three sequence elements define the 3' ss: an AG dinucleotide at the 3' end of the intron, a variable length of pyrimidine nucleotides within the intron called the polypyrimidine tract, and a branch-point sequence upstream of the polypyrimidine tract that generally contains a conserved adenosine. Recognition of these sequences by different components of the spliceosome machinery is required for the initial step of pre-mRNA splicing (Will and Luhrmann, 2011).

SF3B1 encodes subunit 1 of the splicing factor 3b (SF3b) protein complex. Together with the SF3a protein complex and a 12S rRNA, SF3b forms the U2 snRNP (Kramer, 1996). Base pairing between the U2 snRNP and the branch-point sequence is essential for pre-mRNA splicing (Gozani et al., 1998). The SF3b/SF3a complex anchors the U2 snRNP to the pre-mRNA (Gozani et al., 1996), and SF3B1 is a critical component of the activated spliceosome that helps position the branch-point adenosine for nucleophilic attack from the 5' ss (Gozani et al., 1998).

SF3B1 point mutations observed in MDS are confined to exons 14 through 16. The most common SF3B1 mutation is an A-to-G transition that results in a lysine to glutamic acid substitution at amino acid position 700 (K700E) (Papaemmanuil et al., 2011; Yoshida et al., 2011). The absence of nonsense or frameshift mutations and the presence of specific amino acid substitutions in each of the three most commonly mutated spliceosome genes suggest that specific alterations of function are required for their pathogenesis in MDS.

SF3B1 mutations are present in ~25% of all MDS cases (Garcia-Manero, 2012; Malcovati et al., 2011) and in more than 85% of cases of refractory anemia with ring sideroblasts (RARS), a form of MDS characterized by an isolated anemia, erythroid dysplasia, and the presence of at least 15% ring sideroblasts in the bone marrow (Malcovati et al., 2011; Mufti et al., 2008; Papaemmanuil et al., 2011; Vardiman et al., 2002; Yoshida et al., 2011). Ring sideroblasts are erythroid precursors with pathologically iron-laden mitochondria encircling the nucleus (Cartwright and Deiss, 1975; Mufti et al., 2008).

Several studies have attempted to decipher the role of MDS-associated splicing factor mutations in malignant hematopoiesis in vivo. Mouse models of MDS-associated splicing factor mutations in *Srsf2* (Kim et al., 2015) and *U2AF1* (Shirai et al., 2015) exhibit features of MDS, including cytopenias and an increase in hematopoietic stem and progenitor cells (HSPCs). Transcriptome analysis has revealed distinct splicing abnormalities between the two genotypes related to their function within the spliceosome. In this article, we describe a hematopoietic-specific conditional knockin mouse model of *Sf3b1*<sup>K700E</sup> and characterize its effects on malignant hematopoiesis, pre-mRNA splicing, and the pathogenesis of MDS.

## RESULTS

### Physiologic, Hematopoietic-Specific SF3B1<sup>K700E</sup> Expression Causes a Progressive Macrocytic Anemia

To study the role of SF3B1 mutations in the pathogenesis of MDS, we generated an *Sf3b1*<sup>K700E</sup> conditional knockin mouse (Figure 1A). Mice heterozygous for the allele (denoted *Sf3b1*<sup>+/K700E</sup>) were crossed with Mx1-Cre transgenic animals, and expression of Cre recombinase was induced with polyinosine-polycytosine (plpC) injection (Jaisser, 2000; Kuhn et al., 1995). We confirmed recombination by PCR performed on genomic DNA isolated from peripheral blood 3 weeks after plpC injection (Figure 1B). Expression of the A2213G mutation was confirmed by Sanger sequencing of cDNA isolated from peripheral blood (Figure 1C) and by RNA sequencing (RNA-seq) (Figure S1A). We confirmed that total *Sf3b1* expression was similar between wild-type Mx1-Cre-positive littermates (denoted *Sf3b1*<sup>+/+</sup>), *Sf3b1*<sup>+/K700E</sup> mice, and Mx1-Cre-negative mice that carried the targeting construct (denoted Flox Cre Negative) by qRT-PCR (Figure S1B).

We analyzed 11 *Sf3b1*<sup>+/K700E</sup> mice and nine littermate controls for a period of 64 weeks following plpC treatment. Compared with *Sf3b1*<sup>+/+</sup> littermate controls, *Sf3b1*<sup>+/K700E</sup> mice developed a progressive anemia. Anemia was present as early as 4–8 weeks post plpC and was more severe by 20 weeks post plpC (Figure 1D). Macrocytosis, an abnormal increase in the erythrocyte mean corpuscular volume (MCV), was apparent at 20 weeks post plpC (Figure 1E). The total red blood cell number was also consistently lower in *Sf3b1*<sup>+/K700E</sup> mice than in *Sf3b1*<sup>+/+</sup> littermates beginning at 20 weeks post plpC (Figure S1C). In response to the anemia, plasma erythropoietin levels in *Sf3b1*<sup>+/K700E</sup> mice increased as early as 12 weeks post plpC (Figure 1F) and persisted for longer than 60 weeks (Figure S1D). However, the reticulocyte counts in *Sf3b1*<sup>+/K700E</sup> mice remained inappropriately normal over the course of the 64 weeks (Figure S1E). These findings suggest that a red blood cell production defect is associated with SF3B1<sup>K700E</sup> expression. No significant differences were observed in the total white blood cell count, mature white blood cell lineages, or platelet counts between the two groups (Figures S1F–S1H). All of the *Sf3b1*<sup>+/+</sup> mice were alive at 64 weeks post plpC, whereas two of the *Sf3b1*<sup>+/K700E</sup> mice died (18%, Figure S1I). No animals developed acute leukemia.

To determine whether the erythroid-specific effects we observed with SF3B1<sup>K700E</sup> expression are cell intrinsic, we performed noncompetitive bone marrow transplantation experiments. Four weeks after plpC treatment, unfractionated bone marrow from *Sf3b1*<sup>+/K700E</sup> and *Sf3b1*<sup>+/+</sup> CD45.2<sup>+</sup> littermate donors was transplanted into lethally irradiated congenic CD45.1<sup>+</sup> B6.SJL wild-type recipients. Donor chimerism was >95% in both recipient groups over the course of the experiment (Figure S1J). Similar to the phenotype of *Sf3b1*<sup>+/K700E</sup> primary mice, *Sf3b1*<sup>+/K700E</sup> recipient mice developed a macrocytic anemia within 12 weeks after transplantation (Figures 1G and 1H). White blood cell and platelet counts remained normal (Figures S1K and S1L). Taken together, these findings demonstrate that heterozygous expression of SF3B1<sup>K700E</sup> causes a progressive, macrocytic anemia associated with a compensatory increase in plasma erythropoietin levels and relative preservation of the white blood cell and platelet counts.

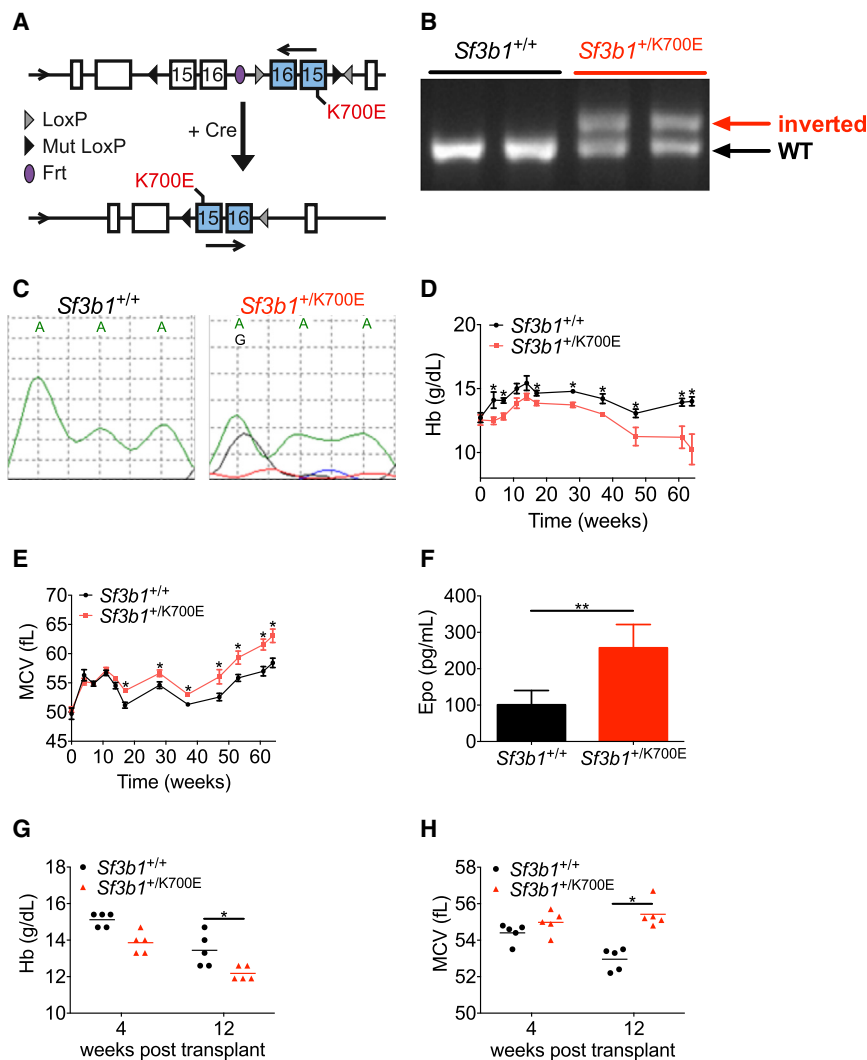


**Figure 1. Heterozygous Conditional Knockin of *Sf3b1*<sup>K700E</sup> Results in a Progressive Macrocytic Anemia**

(A) Targeting allele for conditional expression of *Sf3b1*<sup>K700E</sup>. Upon induction of the Cre recombinase, the inverted exons 15 and 16 containing a guanine mutation at position 2,213 are flipped into the proper orientation.

(B) PCR analysis of genomic DNA isolated from the peripheral blood of two wild-type (*Sf3b1*<sup>+/+</sup>) and two heterozygous mutant (*Sf3b1*<sup>+/K700E</sup>) mice 3 weeks post plpC.

(C) Expression of the A2213G mutation was analyzed by Sanger sequencing of cDNA isolated from the peripheral blood of *Sf3b1*<sup>+/+</sup> and *Sf3b1*<sup>+/K700E</sup> mice 3 weeks post plpC. Data are representative of at least nine mice per group.

(D and E) Analysis of peripheral blood hemoglobin (Hb, D) and mean corpuscular volume (MCV, E) over the course of 64 weeks post plpC (n = 9 *Sf3b1*<sup>+/+</sup> and n = 11 *Sf3b1*<sup>+/K700E</sup> mice).

(F) Plasma erythropoietin (Epo) levels measured 12 weeks post plpC (n = 9 *Sf3b1*<sup>+/+</sup> and n = 11 *Sf3b1*<sup>+/K700E</sup> mice).

(G and H) Peripheral blood Hb (G) and MCV (H) 4 and 12 weeks after noncompetitive transplantation of  $1.0 \times 10^6$  unfractionated bone marrow cells from *Sf3b1*<sup>+/K700E</sup> and *Sf3b1*<sup>+/+</sup> donors into B6.SJL congenic recipient mice (n = 5 mice per group; horizontal line indicates the mean). Data are presented as mean  $\pm$  SEM. \*p < 0.05, \*\*p < 0.001. See also Figure S1.

### **SF3B1<sup>K700E</sup> Expression Is Associated with a Block in Terminal Erythroid Maturation and Erythroid Dysplasia**

To characterize the pathogenesis of the anemia seen in *Sf3b1*<sup>+/K700E</sup> mice, we examined committed erythroid precursor maturation in the spleen and bone marrow of *Sf3b1*<sup>+/+</sup> and *Sf3b1*<sup>+/K700E</sup> mice based on CD71 and Ter119 expression, which subdivides cells into stages R1–R4 of erythroblast maturation (Figure S2A) (Socolovsky et al., 2001; Zhang et al., 2003). We observed a block in erythroblast development, characterized by an accumulation of cells in stage R2 of erythroblast maturation and a concomitant decrease in the stage R4 population in both the spleen (Figure 2A) and bone marrow (Figure S2B) of *Sf3b1*<sup>+/K700E</sup> animals, but not in littermate controls, 64 weeks post plpC. These changes are most prominent in the spleen, the primary site of stress erythropoiesis in mice. We did not observe this block in erythroid maturation in the spleen or bone marrow of young mice (12 weeks post plpC, Figures S2C and S2D), consistent with the onset of primary MDS in older patients (Garcia-Manero, 2012). A similar block in erythroid differentiation was also apparent using a more recently reported methodology for characterizing terminal erythropoiesis (Liu et al., 2013) using

forward scatter, Ter119 expression, and CD44 expression (Figures S2E–S2G).

We next evaluated the effects of the SF3B1<sup>K700E</sup> mutation on stress erythropoiesis by treating mice with phenylhydrazine (PHZ), a drug that induces rapid intravascular hemolysis (Socolovsky et al., 2001). We injected primary *Sf3b1*<sup>+/+</sup> and *Sf3b1*<sup>+/K700E</sup> mice subcutaneously with 30 mg/kg PHZ on days 0 and 1 and then monitored the hemoglobin (Hb) and absolute reticulocyte counts. Experiments were performed on 11-week-old mice, 3 weeks post plpC, to assess stress erythropoiesis at a time when the mice did not have a significant baseline anemia. Following PHZ treatment, the Hb nadir of *Sf3b1*<sup>+/K700E</sup> mice occurred earlier and was significantly lower than the Hb nadir of *Sf3b1*<sup>+/+</sup> controls (Figure 2B). Although not statistically significant, the rise in the reticulocyte count in response to PHZ was lower in *Sf3b1*<sup>+/K700E</sup> mice compared with *Sf3b1*<sup>+/+</sup> mice on days 3 and 6 (Figure S2H). We also assessed erythroblast maturation with CD71 and Ter119 staining, 9 days after PHZ treatment, and noted impaired erythroblast maturation in the spleens of PHZ-treated *Sf3b1*<sup>+/K700E</sup> mice (Figure 2C). This is in contrast to the spleens of similarly aged, young *Sf3b1*<sup>+/K700E</sup> mice that were not treated with PHZ (Figure S2C).

Although several studies have reported that *Sf3b1* heterozygous (*Sf3b1*<sup>+/-</sup>) mice do not develop progressive macrocytic anemia (Matsunawa et al., 2014; Visconte et al., 2012b; Wang et al., 2014), erythroid maturation was only specifically measured

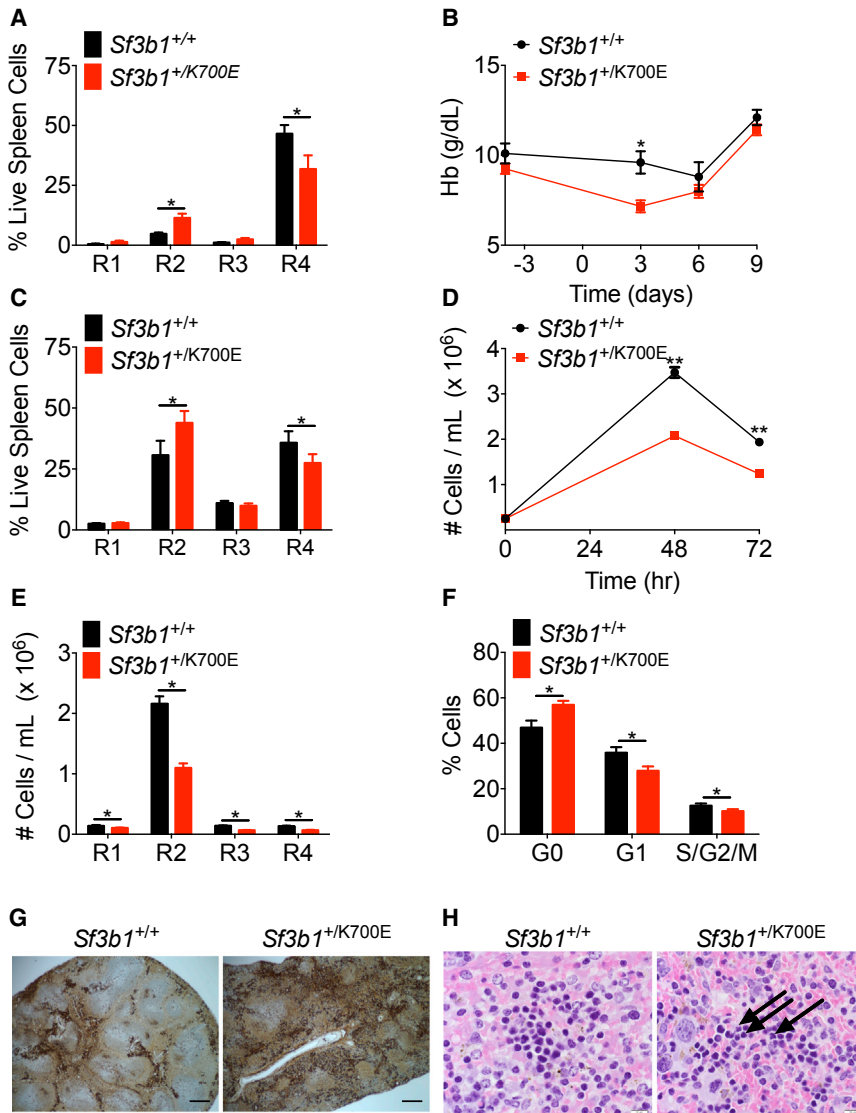


**Figure 2. Heterozygous Conditional Knockin of *Sf3b1*<sup>K700E</sup> Causes a Cell-Intrinsic Block in Terminal Erythroid Maturation and Erythroid Dysplasia**

(A) Analysis of terminal erythroid maturation, defined as progression from immature R1 to more mature R4 erythroblasts, in the spleens of *Sf3b1*<sup>+/+</sup> and *Sf3b1*<sup>+/*K700E*</sup> mice, 64 weeks post plpC (n = 9 *Sf3b1*<sup>+/+</sup> and 11 *Sf3b1*<sup>+/*K700E*</sup> mice).

(B) Hb measured 4 days before and 3, 6, and 9 days after the first injection of *Sf3b1*<sup>+/+</sup> and *Sf3b1*<sup>+/*K700E*</sup> animals with phenylhydrazine (PHZ, n = 11 *Sf3b1*<sup>+/+</sup> and n = 10 *Sf3b1*<sup>+/*K700E*</sup> mice).

(C) Analysis of terminal erythroid maturation in the spleens of 11-week-old *Sf3b1*<sup>+/+</sup> and *Sf3b1*<sup>+/*K700E*</sup> mice, 9 days after PHZ treatment (n = 6 *Sf3b1*<sup>+/+</sup> and n = 5 *Sf3b1*<sup>+/*K700E*</sup> mice).

(D–F) Bone marrow c-Kit<sup>+</sup> progenitor cells (2.0 × 10<sup>5</sup>) from three *Sf3b1*<sup>+/+</sup> and three *Sf3b1*<sup>+/*K700E*</sup> mice were isolated 24 weeks post plpC and plated in erythroid differentiation medium. (D) The number of *Sf3b1*<sup>+/+</sup> or *Sf3b1*<sup>+/*K700E*</sup> cells in culture 48 and 72 hr after plating was quantified in triplicate samples from each mouse. (E) The number of cells in each stage of terminal erythroid maturation 48 hr after plating was quantified in triplicate samples from each mouse. (F) Cell-cycle analysis by combined proliferation (Ki-67) and cell-cycle (Hoechst 33342) staining in permeabilized *Sf3b1*<sup>+/+</sup> or *Sf3b1*<sup>+/*K700E*</sup> cells, 48 hr after cells were plated (G0, Ki-67<sup>+</sup>/Hoechst<sup>-</sup>; G1, Ki67<sup>+</sup>/Hoechst<sup>-</sup>; S/G2/M, Ki-67<sup>+</sup>/Hoechst<sup>+</sup>; duplicate samples were analyzed from three separate mice per group).

(G) Spleens from *Sf3b1*<sup>+/+</sup> and *Sf3b1*<sup>+/*K700E*</sup> mice, 64 weeks post plpC, stained with an anti-CD71 antibody to mark erythroid progenitor cells. Scale bar represents 125 μm.

(H) H&E stains of spleens from *Sf3b1*<sup>+/+</sup> and *Sf3b1*<sup>+/*K700E*</sup> mice, 47 weeks post plpC. Arrows indicate dysplastic erythroid precursors. Scale bar represents 10 μm.

Data are presented as mean ± SEM. \*p < 0.05, \*\*p < 0.01. See also Figure S2.

in one study where no differences were seen (Wang et al., 2011). Visconte et al. (2014) subsequently observed an intermittent increase in MCV and a statistically significant decrease in Hb at 11 months in *Sf3b1*<sup>+/-</sup> mice. We therefore sought to compare *Sf3b1*<sup>+/+</sup> and *Sf3b1*<sup>+/*K700E*</sup> erythroblast maturation using an in vitro culture system that closely mimics the in vivo terminal proliferation and maturation of erythroid cells. Equal numbers of c-Kit<sup>+</sup> HSPCs were isolated from the bone marrow of *Sf3b1*<sup>+/+</sup> and *Sf3b1*<sup>+/*K700E*</sup> mice, and the cells were cultured in the presence of cytokines that induce erythroid differentiation (Ishikawa et al., 2014). Although both the *Sf3b1*<sup>+/+</sup> and *Sf3b1*<sup>+/*K700E*</sup> HSPCs differentiated in culture, the total number of cells (Figure 2D) and the absolute number of cells at each stage of erythroid maturation (Figure 2E) were significantly lower in cells derived from the *Sf3b1*<sup>+/*K700E*</sup> animals compared with *Sf3b1*<sup>+/+</sup> animals. Cell-cycle analysis revealed a significantly lower percentage of *Sf3b1*<sup>+/*K700E*</sup> cells in G1 and a higher percentage of *Sf3b1*<sup>+/*K700E*</sup> cells in G0 compared with

*Sf3b1*<sup>+/+</sup> erythroblasts (Figure 2F). There was no difference in apoptosis based on annexin V staining (Figure S2I). In contrast to the *Sf3b1*<sup>+/*K700E*</sup> HSPCs, in vitro erythroid differentiation of *Sf3b1*<sup>+/-</sup> HSPCs was not impaired (Figures S2J and S2K).

There are also conflicting reports in the literature regarding whether *Sf3b1* haploinsufficiency causes dyserythropoiesis and ring sideroblast formation. Visconte et al. (2012b, 2014) noted rare ring sideroblasts and some dyserythropoietic features in the bone marrow of *Sf3b1*<sup>+/-</sup> mice. In contrast, two independent groups quantified the number of ring sideroblasts in the bone marrow of *Sf3b1*<sup>+/+</sup> and *Sf3b1*<sup>+/-</sup> mice and found no differences between these animals (Matsunawa et al., 2014; Wang et al., 2014). We performed an extensive review of the peripheral blood and bone marrow of *Sf3b1*<sup>+/+</sup> and *Sf3b1*<sup>+/*K700E*</sup> mice and did not find a statistically significant increase in ring sideroblasts or circulating siderocytes, enucleated red blood cells with one or more Perls' stain-positive iron granules, in the *Sf3b1*<sup>+/*K700E*</sup> animals (data not shown). This is consistent with the absence

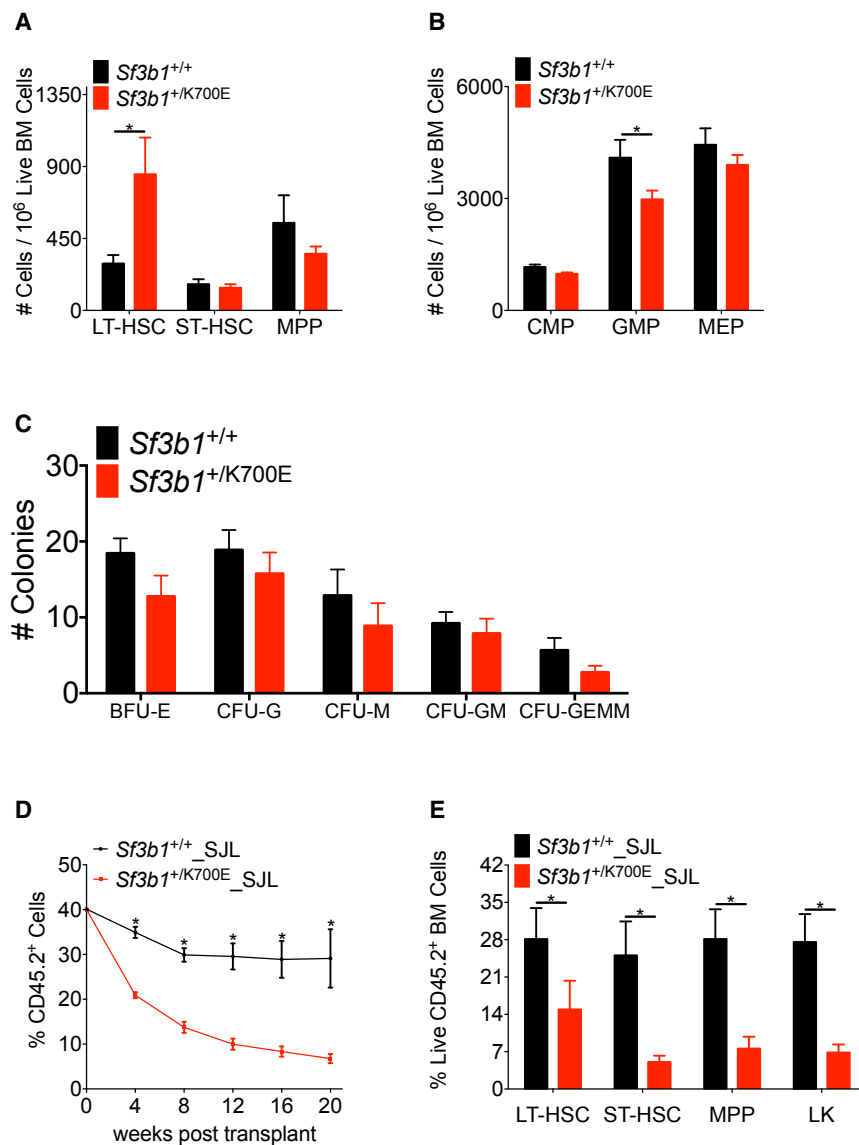


**Figure 3. Heterozygous Expression of SF3B1<sup>K700E</sup> Selectively Enriches for Long-Term Hematopoietic Stem Cells but Is Associated with Decreased Repopulating Ability**

(A and B) Number of LT-HSCs, ST-HSCs, and MPPs (A) and CMPs, GMPs, and MEPs (B) in the bone marrow of *Sf3b1*<sup>+/+</sup> and *Sf3b1*<sup>+/K700E</sup> mice, 64 weeks post plpC (n = 9 *Sf3b1*<sup>+/+</sup> and n = 11 *Sf3b1*<sup>+/K700E</sup> mice).

(C) Absolute number of colonies (BFU-E, CFU-G, CFU-M, CFU-GM, CFU-GEMM) 7 days after 2.0 × 10<sup>5</sup> unfractionated bone marrow cells isolated from *Sf3b1*<sup>+/+</sup> or *Sf3b1*<sup>+/K700E</sup> mice 24 weeks post plpC were plated in M3434 methylcellulose. Triplicate samples were plated from three mice per group.

(D) Percentage of CD45.2 donor chimerism in the peripheral blood 4–20 weeks after competitive repopulation assay. Unfractionated bone marrow cells (1 × 10<sup>6</sup>) from CD45.2<sup>+</sup> *Sf3b1*<sup>+/+</sup> or *Sf3b1*<sup>+/K700E</sup> mice were mixed 1:1 with CD45.1<sup>+</sup> B6.SJL unfractionated bone marrow cells and transplanted into lethally irradiated (10.5 Gy) B6.SJL recipients (n = 5 mice per group). CD45.2 chimerism of the input bone marrow was measured at time 0 (n = 1 sample per group).

(E) Percentage of CD45.2<sup>+</sup> donor LT-HSC, ST-HSC, MPP, and LK chimerism in the bone marrow of *Sf3b1*<sup>+/+</sup> or *Sf3b1*<sup>+/K700E</sup> recipient mice 20 weeks after competitive repopulation assay (n = 4–5 mice per group).

Data are presented as mean ± SEM. \*p < 0.05. See also Figure S3.

of ring sideroblasts in mouse models of congenital sideroblastic anemias, including a conditional knockout model of *Abcb7* (Friedman et al., 2004; Keyhani et al., 1974; Pondarrie et al., 2007). However, we did observe an increase in erythroid precursors and erythroid dysplasia in the spleens of *Sf3b1*<sup>+/K700E</sup> mice (Figures 2G and 2H). No significant differences in bone marrow cellularity were observed between *Sf3b1*<sup>+/+</sup> and *Sf3b1*<sup>+/K700E</sup> mice (data not shown). In aggregate, these data demonstrate that hematopoietic-specific expression of the *Sf3b1*<sup>K700E</sup> allele in mice leads to impaired terminal erythroid maturation, which is exacerbated by age and stress erythropoiesis.

### SF3B1<sup>K700E</sup> Expression Results in Expansion of the Long-Term Hematopoietic Stem Cell Compartment

We next determined whether expression of SF3B1<sup>K700E</sup> during adult hematopoiesis affects different HSPC compartments by performing multi-parameter flow cytometry on the bone marrow of *Sf3b1*<sup>+/+</sup> and *Sf3b1*<sup>+/K700E</sup> mice, 64 weeks after

plpC treatment. Although we found no significant difference in the frequency of Lin<sup>−</sup> Sca-1<sup>+</sup> c-Kit<sup>+</sup> (LSK) cells (data not shown), we observed a significant increase in the frequency of CD150<sup>+</sup> CD48<sup>−</sup> LSK long-term repopulating hematopoietic stem cells (LT-HSCs) and a statistically significant decrease in the percentage of granulocyte/monocyte progenitors (GMPs) in aged *Sf3b1*<sup>+/K700E</sup> mice (Figures 3A and 3B). We observed no significant differences in the frequency of short-term hematopoietic stem cells (ST-HSCs), multi-potent progenitors (MPPs), common myeloid progenitors (CMPs), megakaryocyte/erythroid progenitors (MEPs), or colony-forming units in methylcellulose assays (Figures 3A–3C).

To investigate whether this increase in LT-HSCs was due to increased self-renewal in vivo, we performed competitive repopulation experiments. Four weeks after plpC treatment, 1 million unfractionated bone marrow cells from CD45.2<sup>+</sup> *Sf3b1*<sup>+/K700E</sup> or *Sf3b1*<sup>+/+</sup> littermates were mixed in a 1:1 ratio with unfractionated bone marrow cells from congenic CD45.1<sup>+</sup> B6.SJL mice and injected into lethally irradiated CD45.1<sup>+</sup> B6.SJL recipients. At all time points analyzed, we observed significantly lower peripheral blood chimerism in the *Sf3b1*<sup>+/K700E</sup> recipient mice compared with the *Sf3b1*<sup>+/+</sup> recipient mice (Figure 3D). CD45.2 chimerism was significantly lower in all stem and progenitor cells (Figure 3E), and we did not observe any skewing of mature white blood cells

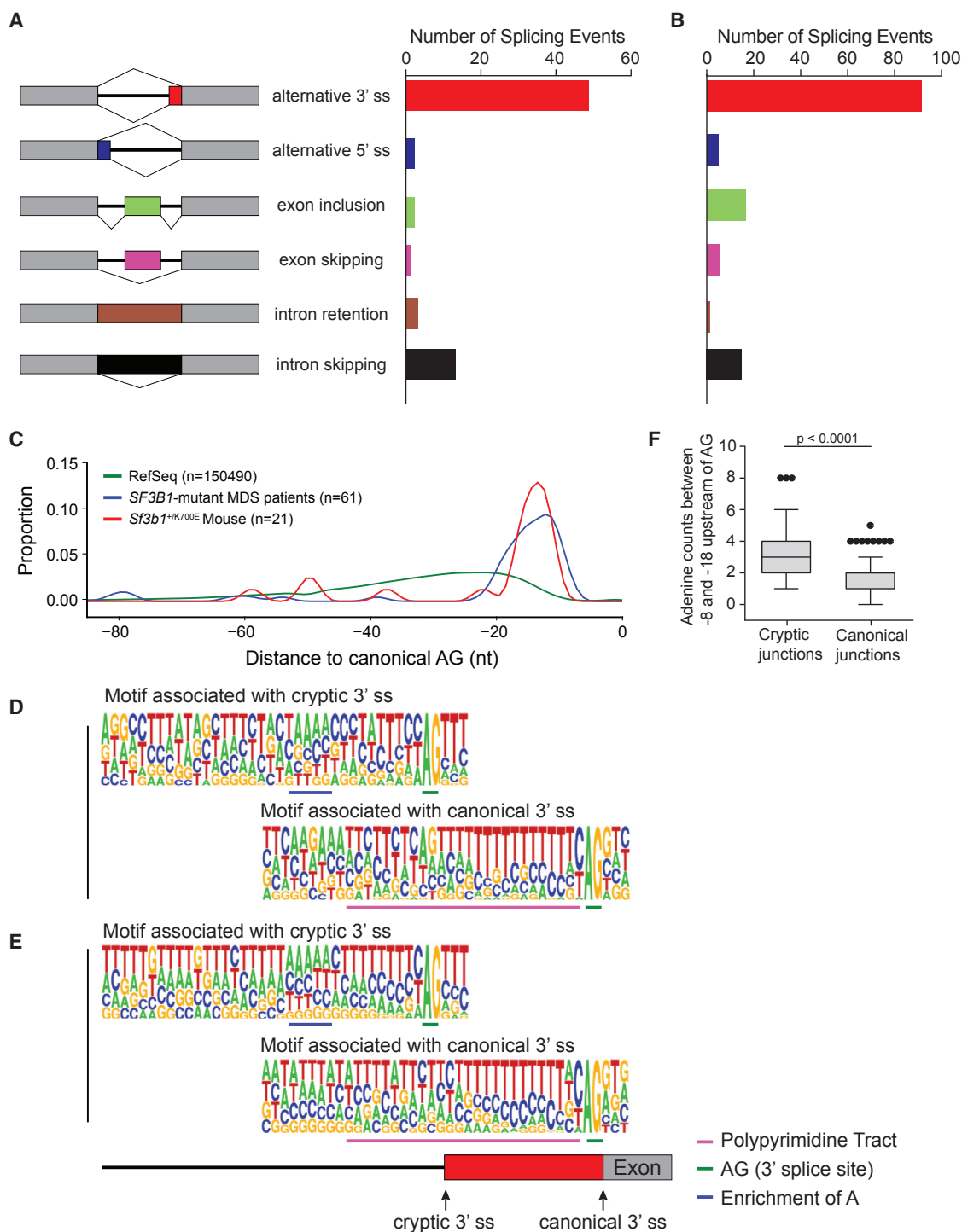


**Figure 4. Aberrant 3' Splicing due to Recognition of an Alternative Branch-Point Adenosine Motif Is Conserved between Murine and Human Cells Expressing Mutant SF3B1**

(A) Number and type of alternative splicing events in *Sf3b1*<sup>+K700E</sup> LK myeloid progenitors compared with littermate controls (three mice per group, n = 72 events; FDR < 0.1).

(B) Number and type of alternative splicing events in unfractionated bone marrow mononuclear cells isolated from *SF3B1*-mutant (n = 6) compared with wild-type *SF3B1* (n = 4) MDS patient samples (n = 134 events; FDR < 0.05).

(C) Density plot of the relative positions of cryptic 3' splice sites (ss) compared with their canonical 3' ss in *SF3B1*-mutant MDS patient samples and *Sf3b1*<sup>+K700E</sup> myeloid progenitors. The distance to the first AG from all reference sequence (RefSeq) canonical 3' ss is included for comparison (n represents the number of alternative 3' splicing events analyzed).

(legend continued on next page)

**Table 1. MDS Patient Sample Characteristics**

Sample ID	SF3B1	Mutant Allele Frequency	Sex	FAB <sup>a</sup>	IPSS <sup>b</sup>	Karyotype	Additional Mutations
MDS_149	–	–	M	RARS	int-1	normal	TET2
MDS_314	p.K700E	42.69	M	RA	int-1	normal	ASXL1
MDS_228	–	–	M	RA	low	normal	ASXL1
MDS_260	p.K666T	44.60	M	RA	low	normal	
MDS_328	–	–	M	RARS	int-1	normal	TET2
MDS_361	p.K700E	38.32	M	RARS	int-1	normal	
MDS_292	–	–	M	RA	low	normal	none
MDS_253	p.K666R	42.62	M	RA	low	normal	
MDS_334	p.K700E	36.81	M	RA	low	normal	
MDS_341	p.K700E	32.82	M	RARS	low	normal	

<sup>a</sup>French-American-British Classification.

<sup>b</sup>MDS International Prognostic Scoring System Score. int-1, intermediate 1.

derived from *Sf3b1*<sup>+/K700E</sup> HSPCs (Figures S3A–S3C). Given the low level of peripheral blood chimerism noted as early as 4 weeks after transplantation, we cannot completely rule out an engraftment defect in the *Sf3b1*<sup>+/K700E</sup> cells. However, we have observed similar engraftment of *Sf3b1*<sup>+/K700E</sup> and *Sf3b1*<sup>+/+</sup> bone marrow cells in noncompetitive transplant experiments (Figure S1J). Taken together, these data suggest that hematopoietic-specific expression of SF3B1<sup>K700E</sup> is associated with an increase in the frequency of immunophenotypic LT-HSCs in the bone marrow, but a significantly impaired capacity to reconstitute hematopoiesis in a competitive transplantation setting, relative to *Sf3b1*<sup>+/+</sup> cells.

### SF3B1<sup>K700E</sup> Expression Leads to Increased Alternative 3' Splice-Site Usage

To determine whether SF3B1<sup>K700E</sup> expression is associated with mutation-specific alterations in pre-mRNA splicing, we performed RNA-seq on myeloid progenitor (Lin<sup>–</sup> c-Kit<sup>+</sup>, LK) cells sorted from three *Sf3b1*<sup>+/K700E</sup> and three *Sf3b1*<sup>+/+</sup> mice, 4 weeks after plpC administration. *Sf3b1*<sup>K700E</sup> mutant allele expression was 27%–32% (Figure S1A). We identified 72 aberrant splicing events that were specific to *Sf3b1*<sup>+/K700E</sup> myeloid progenitors (false discovery rate [FDR] < 0.1), with 48 of 72 (66%) of these events representing alternative 3' splicing events (Figure 4A).

To extend these findings to human samples, we performed RNA-seq on unfractionated bone marrow mononuclear cells isolated from six SF3B1-mutant and four SF3B1-wild-type MDS patient samples matched for MDS subtype, prognostic score, karyotype, and the presence or absence of additional MDS-associated mutations (Table 1). In total, 134 aberrant splicing events were identified in patient samples with SF3B1 mutations (FDR < 0.05, Figure 4B). Although comparison of the differentially spliced genes identified in human SF3B1-mutant

MDS and *Sf3b1*<sup>+/K700E</sup> myeloid progenitor cells revealed minimal overlap (Tables S1 and S2), the types of splicing events were remarkably similar. As observed in murine *Sf3b1*-mutant cells, the most common aberrant splicing event in SF3B1-mutated MDS samples was alternative 3' ss selection (91 of 134, 67.9%; Figure 4B). The locations of the cryptic 3' ss in mouse and human cells were both between –15 and –24 nt upstream of the canonical 3' ss (Figure 4C), similar to recently published reports studying 3' ss selection in other SF3B1-mutant cancers (Alsafadi et al., 2016; Darman et al., 2015; DeBoever et al., 2015). Finally, the sequence contexts associated with the cryptic 3' ss in both the *Sf3b1*<sup>+/K700E</sup> myeloid progenitors (Figure 4D) and SF3B1-mutant MDS patient samples (Figure 4E) are both characterized by upstream adenosine enrichment and a shorter/weaker polypyrimidine tract (Figure 4F and data not shown), motifs which are in accord with mutant SF3B1-specific cryptic ss previously reported in chronic lymphocytic leukemia (CLL) and several solid tumor patient samples and cell lines (Alsafadi et al., 2016; Darman et al., 2015).

Additional computational analysis of the sequences between each cryptic and canonical 3' ss revealed eight genes that were differentially spliced in the presence of mutant SF3B1 in both human and murine cells (FDR < 0.05, Table 2). Three of the cryptic 3' ss were in junctions that were ≥95% conserved between mice and humans. Two of these genes are predicted to be involved in RNA processing: SKIV2L encodes a putative RNA helicase predicted to block translation of poly(A)-deficient mRNA; SERBP1 is predicted to encode an RNA-binding protein with a role in the regulation of mRNA stability.

The lack of overlapping genes between human and murine samples is likely due to the poor conservation of intronic DNA sequences between species (Roy and Gilbert, 2006). This is illustrated by ABCB7, a heme transporter known to be mutated

(D and E) Consensus 3' ss motif near the canonical (bottom) 3' AG dinucleotide and cryptic (top) 3' AG dinucleotide for 21 alternative 3' splicing events identified in *Sf3b1*<sup>+/K700E</sup> compared with *Sf3b1*<sup>+/+</sup> myeloid progenitor cells (D) and 67 alternative 3' splicing events identified in SF3B1-mutant compared with wild-type SF3B1 bone marrow mononuclear cells (E). Motif components are underlined and defined in the key.

(F) The number of adenosines found 8–18 nt upstream of the cryptic AG compared with the canonical AG in six SF3B1-mutant MDS patient samples. Box plots and whiskers are represented as per the Tukey method.

See also Figure S4; Tables S1, S2, and S3.

**Table 2. Genes with Conserved Aberrant 3' Splice Sites between *Sf3b1*<sup>+K700E</sup> Myeloid Progenitors and *SF3B1*-Mutant MDS Patient Samples**

Mouse Aberrant Junction <sup>a</sup>	Mouse Gene Symbol	Human Gene Symbol	Human Aberrant Junction <sup>b</sup>	Mouse NMD <sup>c</sup>	Human NMD
chr1:156041134-156051278:+:start	<i>Tor1aip2</i>	<i>TOR1AIP2</i>	chr1:179835004-179846373:-:end	no	no
chr1:156041002-156051278:+:start	<b><i>Tor1aip2</i></b>	<b><i>TOR1AIP2</i></b>	chr1:179835004-179846373:-:end	no	no
chr1:92918126-92918965:+:start	<i>Rnpepl1</i>	<i>RNPEPL1</i>	chr2:241515027-241516055:+:start	no	yes
chr19:41773142-41774065:-:end	<i>Arhgap19</i>	<i>ARHGAP19</i>	chr10:99023246-99024582:-:end	no	yes
chr17:34846173-34846521:-:end	<i>Skiv2l</i>	<i>SKIV2L</i>	chr6:31936315-31936399:+:start	no	yes
chr6:67272228-67272863:+:start	<b><i>Serbp1</i></b>	<b><i>SERBP1</i></b>	chr1:67890660-67890765:-:end	no	no
chr2:59933730-59935214:-:end	<b><i>Baz2b</i></b>	<b><i>BAZ2B</i></b>	chr2:160253915-160255339:-:end	no	no
chr12:84295335-84297989:+:start	<i>Ptgr2</i>	<i>PTGR2</i>	chr14:74358911-74360478:+:start	ambiguous	no
chr6:67272027-67272138:+:start	<i>Serbp1</i>	<i>SERBP1</i>	chr1:67890660-67890765:-:end	no	no
chr18:36613976-36614714:+:start	<i>Ankhd1</i>	<i>ANKHD1-EIF4EBP3</i>	chr5:139815842-139818078:+:start	no	no

Bold indicates junctions that are  $\geq 95\%$  conserved between mouse and human.

<sup>a</sup>Sequences were aligned to hg19.

<sup>b</sup>Sequences were aligned to mm10.

<sup>c</sup>NMD, aberrant transcript predicted to undergo nonsense-mediated decay.

in X-linked sideroblastic anemia with ataxia (Allikmets et al., 1999) and reported to be downregulated in RARS (Boulwood et al., 2008; Pellagatti et al., 2006). In our human MDS data, we also observed the aberrant splicing of *ABCB7* described by Darman et al. (2015) in an isogenic B cell line expressing the *SF3B1*<sup>K700E</sup> mutation (Figure S4A). However, the sequence for the *ABCB7* cryptic ss is not conserved in mice, and we did not observe aberrant splicing of *Abcb7* in the *Sf3b1*-mutant murine cells.

Gene set enrichment analysis of the differentially expressed genes revealed significant changes in genes involved in RNA processing and metabolism, cell cycle, heme metabolism, and nonsense-mediated decay (NMD, Table S3). NMD was predicted to occur in 36.8% of the altered murine transcripts with an FDR <0.1, and 32.7% of the altered human transcripts with an FDR <0.05 (Tables S1 and S2). Gene-expression analysis of the murine (Figure S4B) and human (Figure S4C) genes with altered transcripts predicted to undergo NMD revealed that their expression was significantly less than the expression of genes with altered transcripts that were not predicted to undergo NMD ( $p = 0.0003$ ). These data demonstrate that *Sf3b1*<sup>+K700E</sup> myeloid progenitors and *SF3B1*-mutant MDS samples faithfully recapitulate the alterations in pre-mRNA splicing observed in other cancer cells with *SF3B1* mutations.

#### Additive Effect of *Sf3b1*<sup>K700E</sup> Mutation and *Tet2* Deletion on MDS Pathogenesis

Loss-of-function mutations in *TET2* occur in more than 20% of MDS patient samples (Bejar et al., 2011; Langemeijer et al., 2009), and *SF3B1* and *TET2* mutations commonly co-occur in patients with MDS (Bejar et al., 2012; Haferlach et al., 2014). To study the effect of this combination of mutations on MDS pathogenesis, we crossed *Sf3b1*<sup>+K700E</sup> mice with a previously characterized conditional *Tet2* knockout mouse (Moran-Crusio et al., 2011; Quivoron et al., 2011).

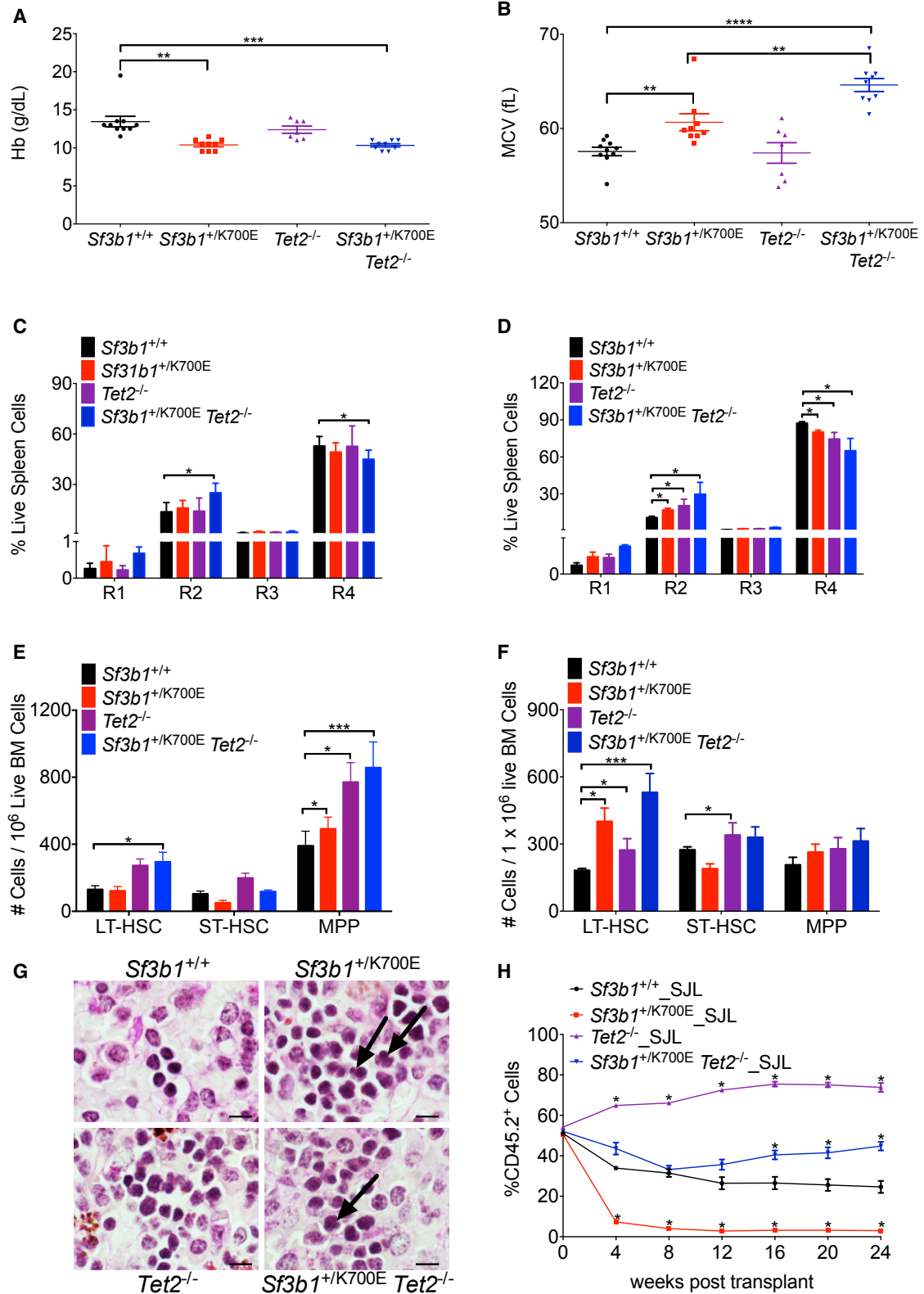
Both *Sf3b1*<sup>+K700E</sup> and *Sf3b1*<sup>+K700E</sup> *Tet2*<sup>-/-</sup> mice developed a progressive macrocytic anemia (Figures 5A and 5B), with *Sf3b1*<sup>+K700E</sup> *Tet2*<sup>-/-</sup> mice exhibiting a more severe anemia

and macrocytosis. Moreover, the double-mutant mice display an accelerated terminal erythroid maturation block compared with mice harboring either mutation alone, as early as 12 weeks post plpC (Figure 5C). By 45 weeks post plpC, this block in erythroid maturation is apparent in all of the mutant animals (Figure 5D).

Analysis of mature white blood cells at 45 weeks post plpC was notable for an increased percentage of granulocytes associated with homozygous *Tet2* loss. A statistically significant increase in the percentage of granulocytes was noted in the peripheral blood of *Tet2*<sup>-/-</sup> mice (Figure S5A). Compared with *Sf3b1*<sup>+/+</sup> and *Sf3b1*<sup>+K700E</sup> mice, both *Tet2*<sup>-/-</sup> and *Sf3b1*<sup>+K700E</sup> *Tet2*<sup>-/-</sup> mice had a statistically significant increase in the percentage of granulocytes and a statistically significant decrease in the percentage of B cells in both the spleen (Figure S5B) and the bone marrow (Figure S5C).

At 12 weeks, we found a small but reproducible increase in the frequency of LT-HSCs in *Sf3b1*<sup>+K700E</sup> *Tet2*<sup>-/-</sup> mice compared with *Sf3b1*<sup>+/+</sup> mice (Figure 5E). By 45 weeks this expansion of LT-HSCs in *Sf3b1*<sup>+K700E</sup> *Tet2*<sup>-/-</sup> mice was more marked when compared with the increase observed in *Sf3b1*<sup>+K700E</sup> ( $p = 0.028$ ) or *Tet2*<sup>-/-</sup> ( $p = 0.00768$ ) mice (Figure 5F). The spleens of *Sf3b1*<sup>+K700E</sup> *Tet2*<sup>-/-</sup> mice were enlarged, similar to those of *Tet2*<sup>-/-</sup> mice (Figure S5D). Consistent with an additive effect of these mutations on MDS pathogenesis, histopathological analysis of the spleens of the double-mutant animals was notable for dysplastic erythroid progenitors and megakaryocytes (Figure 5G). We did not observe a statistically significant decrease in survival in the double-mutant animals (Figure S5E), and none of the animals developed leukemia during the course of these experiments.

We next compared the function of double-mutant and single-mutant stem cells in competitive repopulation experiments. Four weeks after plpC administration, a one-to-one ratio of *Sf3b1*<sup>+/+</sup>, *Sf3b1*<sup>+K700E</sup>, *Tet2*<sup>-/-</sup>, or *Sf3b1*<sup>+K700E</sup> *Tet2*<sup>-/-</sup> to congenic B6.SJL unfractionated bone marrow was transplanted into lethally irradiated B6.SJL recipients. In contrast to the *Sf3b1*<sup>+K700E</sup> bone marrow recipients, the initial chimerism of



(legend on next page)

*Sf3b1*<sup>+/K700E</sup> *Tet2*<sup>-/-</sup> recipients was similar to that of *Sf3b1*<sup>+/+</sup> recipients (Figure 5H). In addition, the peripheral blood chimerism in *Sf3b1*<sup>+/K700E</sup> *Tet2*<sup>-/-</sup> recipients increased over time with a delayed onset, but similar slope, compared with *Tet2*<sup>-/-</sup> recipients. Analysis of mature lineages was notable for a multi-lineage competitive advantage in *Tet2*<sup>-/-</sup> recipients, as reported previously (Quivoron et al., 2011); however, *Sf3b1*<sup>+/K700E</sup> *Tet2*<sup>-/-</sup> recipients showed myeloid skewing that was most notable in the peripheral blood and spleen (Figure S5F–S5H). Flow cytometric analysis of the stem and progenitor cells 24 weeks after transplantation demonstrated increasing donor chimerism in *Sf3b1*<sup>+/K700E</sup> *Tet2*<sup>-/-</sup> recipient mice as their bone marrow cells matured from LT-HSCs (46.5% CD45.2<sup>+</sup> cells) to more committed myeloid progenitors (80%–90% CD45.2<sup>+</sup> cells; Figures S5I and S5J). This is in contrast to *Tet2*<sup>-/-</sup> recipients that had nearly 100% donor chimerism in all stem and progenitor cell compartments by 24 weeks and *Sf3b1*<sup>+/K700E</sup> bone marrow recipients that had low levels of donor chimerism in all stem and progenitor cell compartments.

Taken together, these data demonstrate that *Tet2* loss exacerbates the macrocytic anemia and impaired terminal erythroid maturation caused by SF3B1<sup>K700E</sup> expression and causes an earlier expansion of LT-HSCs in the double-mutant bone marrow. Furthermore, loss of *Tet2* rescues the impaired competitive repopulating activity conferred by *Sf3b1*<sup>+/K700E</sup>. These phenotypes of the *Sf3b1*<sup>+/K700E</sup> *Tet2*<sup>-/-</sup> mice faithfully recapitulate cardinal features of MDS (Beachy and Aplan, 2010).

### Cells Expressing SF3B1<sup>K700E</sup> Have an Increased Sensitivity to Therapeutic Spliceosome Modulation

Screens to identify naturally occurring products with anti-tumor activity led to the identification of microbial products that specifically inhibit SF3b complex function (Kaida et al., 2007; Kotake et al., 2007; Mizui et al., 2004; Nakajima et al., 1996a, 1996b). E7107 is a derivative of naturally occurring pladienolides that has been shown to inhibit spliceosome assembly (Eskens et al., 2013; Folco et al., 2011; Hong et al., 2014). As splicing factor mutations are uniformly heterozygous and mutually exclusive (Yoshida et al., 2011), we hypothesized that survival of *Sf3b1*-mutant cells may be dependent on the activity of the residual wild-type *Sf3b1* allele and that cells heterozygous for *Sf3b1* mutations may therefore have increased sensitivity to spliceosome modulators.

We tested this hypothesis in vitro using c-Kit<sup>+</sup> HSPCs isolated from the bone marrow of *Sf3b1*<sup>+/+</sup> or *Sf3b1*<sup>+/K700E</sup> mice. We treated the cells with E7107 for 72 hr and observed that although

*Sf3b1*<sup>+/+</sup> murine HSPCs are sensitive to nanomolar concentrations of E7107 (IC<sub>50</sub> = 1.249 nM), *Sf3b1*<sup>+/K700E</sup> HSPCs are sensitive to even lower concentrations of the drug (IC<sub>50</sub> = 0.619 nM, Figure 6A).

To evaluate the activity of E7107 against *Sf3b1*<sup>+/K700E</sup> HSPCs in vivo, we treated competitive transplant recipients with E7107 for a total of 10 days (Figure 6B). Lethally irradiated B6.SJL mice were transplanted with a 1:20 ratio of B6.SJL to either *Sf3b1*<sup>+/+</sup> or *Sf3b1*<sup>+/K700E</sup> unfractionated bone marrow. We assessed initial engraftment 4 weeks after transplantation and found that the peripheral blood CD45.2 chimerism was above 50% in both recipient groups, although lower in the *Sf3b1*<sup>+/K700E</sup> recipients (Figure 6C). We observed a statistically significant decrease in CD45.2 chimerism in the peripheral blood, bone marrow, and spleens of *Sf3b1*<sup>+/K700E</sup> recipients treated with E7107 compared with those treated with vehicle alone (Figures 6C, 6D, and S6A). A similar decrease in chimerism was not seen in *Sf3b1*<sup>+/+</sup> recipients treated with E7107. Treatment of *Sf3b1*<sup>+/K700E</sup> recipients with E7107 was also associated with a statistically significant decrease in lymphoid and myeloid CD45.2 chimerism, LK chimerism, and a lower, though not statistically significant decrease in LSK chimerism (Figures S6B, 6E, and 6F). Taken together, these data show that HSPCs expressing mutant SF3B1 have an increased sensitivity to pharmacologic spliceosome modulation compared with wild-type HSPCs.

### DISCUSSION

We demonstrate that heterozygous, hematopoietic-restricted expression of SF3B1<sup>K700E</sup> is sufficient to cause characteristic features of MDS, including a macrocytic anemia due to a block in terminal erythropoiesis, erythroid dysplasia, and expansion of LT-HSCs in the bone marrow. The finding that SF3B1 mutations in patients with MDS are uniformly heterozygous missense mutations at highly restricted amino acid residues, rather than a range of inactivating mutations, suggests that these mutations confer an alteration of function instead of a loss of protein function. RNA-seq of *Sf3b1*<sup>+/K700E</sup> myeloid progenitor cells and SF3B1-mutant bone marrow mononuclear cells from MDS patients showed that mutant SF3B1 expression is most commonly associated with aberrant 3' mRNA splicing. The motif associated with the cryptic 3' ss is conserved between SF3B1-mutant human and murine samples and is characterized by an enrichment of adenosines and a short polypyrimidine tract upstream of the cryptic 3' ss. This splicing abnormality has also been reported in SF3B1-mutant CLL samples and solid tumors including breast

### Figure 5. The Combination of the *Sf3b1*<sup>K700E</sup> Mutation and *Tet2* Deletion Causes an Earlier Onset of MDS Characteristics and Rescues the Competitive Disadvantage of *Sf3b1*<sup>+/K700E</sup> Stem Cells

(A and B) Peripheral blood Hb (A) and MCV (B) from *Sf3b1*<sup>+/+</sup>, *Sf3b1*<sup>+/K700E</sup>, *Tet2*<sup>-/-</sup>, and *Sf3b1*<sup>+/K700E</sup> *Tet2*<sup>-/-</sup> mice 45 weeks post plpC (n = 7–10 mice per group). (C and D) Analysis of terminal erythroid maturation in the spleens of *Sf3b1*<sup>+/+</sup>, *Sf3b1*<sup>+/K700E</sup>, *Tet2*<sup>-/-</sup>, and *Sf3b1*<sup>+/K700E</sup> *Tet2*<sup>-/-</sup> mice 12 (C) and 45 (D) weeks post plpC (n = 7–10 mice per group).

(E and F) Number of LT-HSCs, ST-HSCs, and MPPs in the bone marrow of *Sf3b1*<sup>+/+</sup>, *Sf3b1*<sup>+/K700E</sup>, *Tet2*<sup>-/-</sup>, and *Sf3b1*<sup>+/K700E</sup> *Tet2*<sup>-/-</sup> mice 12 (E) and 45 (F) weeks post plpC (n = 7–10 mice per group).

(G) Periodic acid-Schiff-stained spleens from *Sf3b1*<sup>+/+</sup>, *Sf3b1*<sup>+/K700E</sup>, *Tet2*<sup>-/-</sup>, and *Sf3b1*<sup>+/K700E</sup> *Tet2*<sup>-/-</sup> mice, 45 weeks post plpC. Arrows indicate dysplastic erythroid precursors. Scale bar represents 5 μm.

(H) Percentage of CD45.2 donor chimerism in the peripheral blood 4–24 weeks after competitive repopulation assay with 1:1 unfractionated bone marrow from *Sf3b1*<sup>+/+</sup>, *Sf3b1*<sup>+/K700E</sup>, *Tet2*<sup>-/-</sup>, or *Sf3b1*<sup>+/K700E</sup> *Tet2*<sup>-/-</sup> CD45.2<sup>+</sup> mice and CD45.1<sup>+</sup> B6.SJL mice transplanted into lethally irradiated B6.SJL recipients (n = 5 mice per group). CD45.2 chimerism of the input bone marrow was measured at time 0 (n = 1 sample per group).

Data are presented as mean ± SEM. \*p < 0.05, \*\*p < 0.01, \*\*\*p < 0.001, \*\*\*\*p < 0.0001. See also Figure S5.

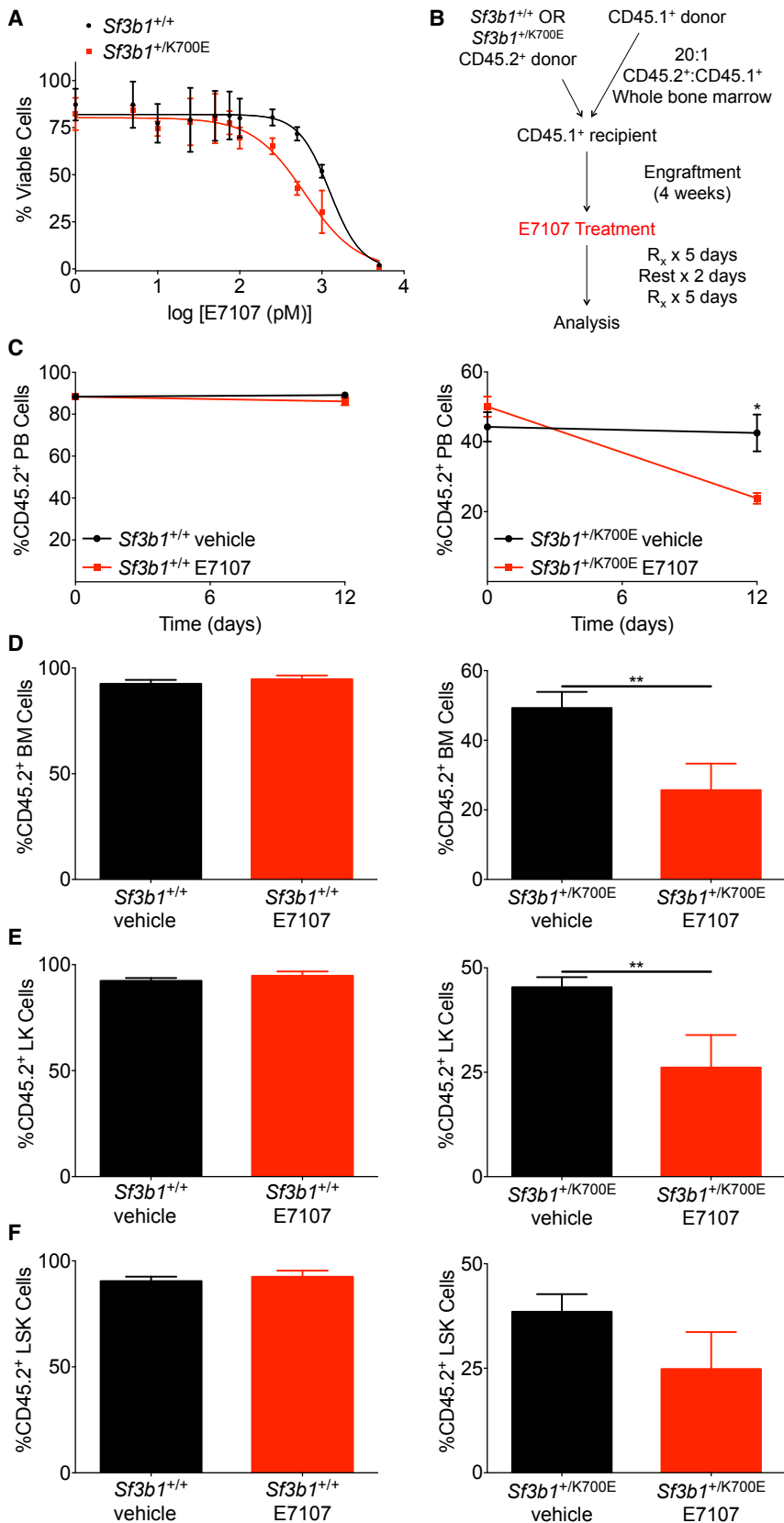


**Figure 6. SF3B1<sup>K700E</sup>-Expressing Cells Are Sensitive to the Spliceosome Modulator, E7107, In Vitro and In Vivo**

(A) c-Kit<sup>+</sup> bone marrow HSPCs ( $2.0 \times 10^4$ ) were isolated from *Sf3b1*<sup>+/+</sup> and *Sf3b1*<sup>+/K700E</sup> mice and cultured in DMSO or increasing concentrations of E7107. Cell viability was assessed using CellTiter-Glo (n = 2 mice per group; triplicate samples per dose). Data are representative of at least five independent experiments with cells harvested 4 to 24 weeks post plpC.

(B) Schematic of in vivo E7107 treatment.

(C) The percentage of CD45.2 donor chimerism in the peripheral blood (PB) of B6.SJL recipient mice transplanted with a 20:1 ratio of *Sf3b1*<sup>+/+</sup> or *Sf3b1*<sup>+/K700E</sup> to B6.SJL unfractionated bone marrow 4 weeks after competitive transplantation (day 0) and 12 days after treatment with E7107 or vehicle (n = 5 mice per group).

(D–F) Unfractionated bone marrow (D), LK myeloid progenitor (E), and LSK (F) CD45.2 donor chimerism in *Sf3b1*<sup>+/+</sup> or *Sf3b1*<sup>+/K700E</sup> recipients treated with E7107 or vehicle as indicated (n = 5 mice per group). Data are presented as mean ± SEM. \*p < 0.05, \*\*p < 0.01. See also Figure S6.

carcinoma and melanoma (Alsafadi et al., 2016; Darman et al., 2015).

The hematopoietic phenotype of the *Sf3b1*<sup>+/K700E</sup> conditional knockin mouse is distinct from that reported in studies of heterozygous deletion of *Sf3b1* (Matsunawa et al., 2014; Visconte et al., 2012b, 2014; Wang et al., 2014). Haploinsufficiency of *Sf3b1* is not associated with anemia, a block in terminal erythroid maturation, or statistically significant differences in HSPC frequencies in mice followed for up to 70 weeks (Matsunawa et al., 2014; Wang et al., 2014). We did not observe substantial numbers of ring sideroblasts in the bone marrow of *Sf3b1*<sup>+/K700E</sup> animals, as seen in MDS patients with *SF3B1* mutations. Murine models of other genetic mutations that lead to sideroblastic anemia in humans also do not produce ring sideroblasts in mice, including loss of *Abcb7* (Friedman et al., 2004; Keyhani et al., 1974; Pondarre et al., 2007).

We found that more than 30% of both the murine and human genes with aberrant splicing associated with *SF3B1* mutations were predicted to undergo NMD. Genes predicted to undergo NMD had decreased expression compared with genes that were not predicted to undergo NMD. Of note, the splicing abnormality in *SF3B1*-mutant cancers is distinct from the aberrant splicing associated with mutations in *Srsf2* (Kim et al., 2015) and *U2AF1* (Shirai et al., 2015). This may contribute to the mutual exclusivity as well as the MDS subtype specificity of splicing factor mutations in MDS.

As *SF3B1* and *TET2* mutations co-occur in patients with MDS (Bejar et al., 2012; Haferlach et al., 2014), we generated double-mutant mice to evaluate the effect of the combination of these mutations. We found that *Sf3b1*<sup>+/K700E</sup> *Tet2*<sup>-/-</sup> mice develop an earlier and more pronounced anemia, a more profound and accelerated expansion of the LT-HSC compartment, and erythroid and megakaryocyte dysplasia. We also found that the combination of *Tet2* loss and *SF3B1*<sup>K700E</sup> expression is sufficient to rescue the competitive repopulation disadvantage induced by expression of *SF3B1*<sup>K700E</sup> alone. The additive effects of *Tet2* loss and *SF3B1*<sup>K700E</sup> expression on the HSPCs from the double-mutant animals may explain why mutations in both of these genes are well tolerated in MDS patient samples.

Finally, we demonstrated that HSPCs expressing *SF3B1*<sup>K700E</sup> have an increased sensitivity to the spliceosome modulator, E7107, both in vitro and in vivo. *Sf3b1* mutation therefore sensitizes cells to pharmacologic targeting of wild-type *SF3B1*, consistent with the observation that the growth of *SF3B1*-mutant endometrial cancer and uveal melanoma cell lines is impaired by deletion of wild-type, but not mutant, *SF3B1* (Zhou et al., 2015). These findings suggest that there may be a therapeutic window for the use of spliceosome modulators in the treatment of hematologic malignancies with *SF3B1* mutations.

## EXPERIMENTAL PROCEDURES

### Generation of an *Sf3b1*<sup>K700E</sup> Conditional Knockin Mouse

Generation of the *Sf3b1*<sup>K700E</sup> conditional knockin mouse is described in Supplemental Experimental Procedures. All experiments and procedures were conducted in the Boston Children's Hospital animal facility and were approved by the Boston Children's Hospital Institutional Animal Care and Use Committee.

### Patient Samples and Sequencing

Patients included in the RNA-seq were diagnosed between 1994 and 2008. Patients were diagnosed with MDS according to the French-American-British

and 2008 World Health Organization classifications. Samples were de-identified at the time of inclusion. This study was approved by the Columbia University Institutional Review Board and performed in accordance with the Declaration of Helsinki. All patients gave their informed written consent. RNA-seq was performed using paired-end reads generated from cDNA libraries prepared from MDS samples (bone marrow mononuclear cells).

### RNA-Seq and Analysis

For sorted mouse cell populations and MDS samples, RNA was extracted using a PrepEase RNA Spin Kit (Affymetrix). For mouse RNAs, nondirectional libraries were prepared using the NEBNext Ultra RNA (poly A) Library Preparation Kit for Illumina (New England Biolabs). DNA fragments of 300 bp were isolated and sequenced on the NextSeq PE150 chip. For MDS samples, cDNA library preparation, sequencing, and raw read filtering methods were executed at BGI as described previously (Ren et al., 2012). Quantification of RNA-seq data, identification of differentially spliced junctions, and motif analysis were conducted as described previously (Darman et al., 2015).

### E7107 Drug Treatment

Increasing concentrations of E7107 (H3 Biomedicine) were added to 20,000 c-Kit<sup>+</sup> cells per well cultured in 96-well plates. Cells were cultured in StemSpan Serum-Free Expansion Medium (STEMCELL Technologies) supplemented with 50 ng/mL m-tpo and 50 ng/mL m-scf. In vivo drug treatment was performed via daily intravenous tail-vein injection of 4 mg/kg/dose E7107 or vehicle (10% ethanol, 5% Tween 80, and saline) for 10 days (5 days on, 2 days off, then repeat). Treated mice were lethally irradiated (10.5 Gy) and transplanted with a 20:1 ratio of *Sf3b1*<sup>+/+</sup> or *Sf3b1*<sup>+/K700E</sup> BL6 unfractionated bone marrow to B6.SJL unfractionated bone marrow. Four weeks after transplantation, peripheral blood CD45.2 chimerism was assessed. Four hours after the last drug treatment, peripheral blood cells, splenocytes, and bone marrow cells were isolated and the donor cell chimerism was again assessed.

### Statistical Analyses

All data are reported as mean ± SEM. We performed analysis for statistically significant differences with the two-tailed Student's t test and one-way ANOVA. Box plots and whiskers are presented as per the Tukey method where the center is the median, and the first and third quartiles define the top and bottom parts of the box. Interquartile range (IQR) is third quartile minus the first quartile (the box). Outliers are defined as 1.5 × IQR outside the first and third quartiles. All flow cytometry data were analyzed with FlowJo Software.

### ACCESSION NUMBERS

The accession number for the RNA sequencing data reported in this paper is GEO: GSE85712.

### SUPPLEMENTAL INFORMATION

Supplemental Information includes Supplemental Experimental Procedures, six figures, and three tables and can be found with this article online at <http://dx.doi.org/10.1016/j.ccell.2016.08.006>.

### AUTHOR CONTRIBUTIONS

E.A.O., A.M., S.B., P.J.S., M.D.F., and B.L.E. designed the study. A.M. and C.J.W. helped generate mice. E.A.O., R.C., D.R.C., A.M.L., A.M., and M.E.C. performed experiments and generated mice. E.A.O. and B.L.E. analyzed and interpreted the data. L.Y. and M.S. performed the RNA-seq analysis. A.M.A. and A.R. provided primary patient MDS samples. S.B. and P.G.S. provided reagents and expertise for the spliceosome modulator experiments. C.J.W., L.W., and R.G.G. provided reagents and expertise. E.A.O., M.D.F., and B.L.E. prepared the manuscript. All authors provided critical review of the manuscript.

### ACKNOWLEDGMENTS

We gratefully acknowledge Ronald Mathieu and Mahnaz Paktinat from the Harvard Stem Cell Institute/Boston Children's Hospital Flow Cytometry Core

Facility, and Renee Rubio and Yaoyu Wang from the Center for Cancer Computational Biology at the Dana-Farber Cancer Institute. We thank Edwin Chen, Julie Losman, Takahiro Maeda, Mohandas Narla, Rafael Bejar, Stanley Lee, Andrew Guirguis, and Damien Wilpitz for their scientific insights and critical review of the manuscript. This work was supported by the NIH (R01 HL082945), the Leukemia and Lymphoma Society, and a STARR Cancer Consortium award to B.L.E. and the NIH R24 DK099808 award to M.D.F. and B.L.E. E.A.O. was supported by an American Society of Hematology/Robert Wood Johnson Foundation Harold Amos Medical Faculty Development Award. S.B., L.Y., M.S., and P.G.S. are full-time employees of H3 Biomedicine. B.L.E. is a consultant for H3 Biomedicine.

Received: December 2, 2015

Revised: April 29, 2016

Accepted: August 16, 2016

Published: September 12, 2016

## REFERENCES

- Allikmets, R., Raskind, W.H., Hutchinson, A., Schueck, N.D., Dean, M., and Koeller, D.M. (1999). Mutation of a putative mitochondrial iron transporter gene (ABC7) in X-linked sideroblastic anemia and ataxia (XLSA/A). *Hum. Mol. Genet.* **8**, 743–749.
- Alsafadi, S., Houy, A., Battistella, A., Popova, T., Wassef, M., Henry, E., Tirode, F., Constantinou, A., Piperno-Neumann, S., Roman-Roman, S., et al. (2016). Cancer-associated SF3B1 mutations affect alternative splicing by promoting alternative branchpoint usage. *Nat. Commun.* **7**, 10615.
- Beachy, S.H., and Aplan, P.D. (2010). Mouse models of myelodysplastic syndromes. *Hematol. Oncol. Clin. North Am.* **24**, 361–375.
- Becerra, S., Andres-Leon, E., Prieto-Sanchez, S., Hernandez-Munain, C., and Sune, C. (2015). Prp40 and early events in splice site definition. *Wiley Interdiscip. Rev. RNA* **7**, 17–32.
- Bejar, R., Stevenson, K., Abdel-Wahab, O., Galili, N., Nilsson, B., Garcia-Manero, G., Kantarjian, H., Raza, A., Levine, R.L., Neuberg, D., and Ebert, B.L. (2011). Clinical effect of point mutations in myelodysplastic syndromes. *N. Engl. J. Med.* **364**, 2496–2506.
- Bejar, R., Stevenson, K.E., Caughey, B.A., Abdel-Wahab, O., Steensma, D.P., Galili, N., Raza, A., Kantarjian, H., Levine, R.L., Neuberg, D., et al. (2012). Validation of a prognostic model and the impact of mutations in patients with lower-risk myelodysplastic syndromes. *J. Clin. Oncol.* **30**, 3376–3382.
- Boulton, J., Pellagatti, A., Nikpour, M., Pushkaran, B., Fidler, C., Cattani, H., Littlewood, T.J., Malcovati, L., Della Porta, M.G., et al. (2008). The role of the iron transporter ABCB7 in refractory anemia with ring sideroblasts. *PLoS One* **3**, e1970.
- Cartwright, G.E., and Deiss, A. (1975). Sideroblasts, siderocytes, and sideroblastic anemia. *N. Engl. J. Med.* **292**, 185–193.
- Chen, M., and Manley, J.L. (2009). Mechanisms of alternative splicing regulation: insights from molecular and genomics approaches. *Nat. Rev. Mol. Cell Biol.* **10**, 741–754.
- Darman, R.B., Seiler, M., Agrawal, A.A., Lim, K.H., Peng, S., Aird, D., Bailey, S.L., Bhavsar, E.B., Chan, B., Colla, S., et al. (2015). Cancer-associated SF3B1 hotspot mutations induce cryptic 3' splice site selection through use of a different branch point. *Cell Rep.* **13**, 1033–1045.
- DeBoever, C., Ghia, E.M., Shepard, P.J., Rassenti, L., Barrett, C.L., Jepsen, K., Jamieson, C.H., Carson, D., Kipps, T.J., and Frazer, K.A. (2015). Transcriptome sequencing reveals potential mechanism of cryptic 3' splice site selection in SF3B1-mutated cancers. *PLoS Comput. Biol.* **11**, e1004105.
- Eskens, F.A., Ramos, F.J., Burger, H., O'Brien, J.P., Piera, A., de Jonge, M.J., Mizui, Y., Wiemer, E.A., Carreras, M.J., Baselga, J., and Tabernero, J. (2013). Phase I pharmacokinetic and pharmacodynamic study of the first-in-class spliceosome inhibitor E7107 in patients with advanced solid tumors. *Clin. Cancer Res.* **19**, 6296–6304.
- Folco, E.G., Coil, K.E., and Reed, R. (2011). The anti-tumor drug E7107 reveals an essential role for SF3b in remodeling U2 snRNP to expose the branch point-binding region. *Genes Dev.* **25**, 440–444.
- Friedman, J.S., Lopez, M.F., Fleming, M.D., Rivera, A., Martin, F.M., Welsh, M.L., Boyd, A., Doctrow, S.R., and Burakoff, S.J. (2004). SOD2-deficiency anemia: protein oxidation and altered protein expression reveal targets of damage, stress response, and antioxidant responsiveness. *Blood* **104**, 2565–2573.
- Garcia-Manero, G. (2012). Myelodysplastic syndromes: 2012 update on diagnosis, risk-stratification, and management. *Am. J. Hematol.* **87**, 692–701.
- Gozani, O., Feld, R., and Reed, R. (1996). Evidence that sequence-independent binding of highly conserved U2 snRNP proteins upstream of the branch site is required for assembly of spliceosomal complex. *Genes Dev.* **10**, 233–243.
- Gozani, O., Potashkin, J., and Reed, R. (1998). A potential role for U2AF-SAP 155 interactions in recruiting U2 snRNP to the branch site. *Mol. Cell Biol.* **18**, 4752–4760.
- Haferlach, T., Nagata, Y., Grossmann, V., Okuno, Y., Bacher, U., Nagae, G., Schnittger, S., Sanada, M., Kon, A., Alpermann, T., et al. (2014). Landscape of genetic lesions in 944 patients with myelodysplastic syndromes. *Leukemia* **28**, 241–247.
- Hong, D.S., Kurzrock, R., Naing, A., Wheeler, J.J., Falchook, G.S., Schiffman, J.S., Faulkner, N., Pilat, M.J., O'Brien, J., and LoRusso, P. (2014). A phase I, open-label, single-arm, dose-escalation study of E7107, a precursor messenger ribonucleic acid (pre-mRNA) spliceosome inhibitor administered intravenously on days 1 and 8 every 21 days to patients with solid tumors. *Invest. New Drugs* **32**, 436–444.
- Ishikawa, Y., Maeda, M., Pasham, M., Aguet, F., Tacheva-Grigorova, S.K., Masuda, T., Yi, H., Lee, S.U., Xu, J., Teruya-Feldstein, J., et al. (2014). Role of the clathrin adaptor PICALM in normal hematopoiesis and polycythemia vera pathophysiology. *Haematologica* **100**, 439–451.
- Jaisser, F. (2000). Inducible gene expression and gene modification in transgenic mice. *J. Am. Soc. Nephrol.* **11** (Suppl 16), S95–S100.
- Kaida, D., Motoyoshi, H., Tashiro, E., Nojima, T., Hagiwara, M., Ishigami, K., Watanabe, H., Kitahara, T., Yoshida, T., Nakajima, H., et al. (2007). Spliceostatin A targets SF3b and inhibits both splicing and nuclear retention of pre-mRNA. *Nat. Chem. Biol.* **3**, 576–583.
- Keyhani, M., Giuliani, D., Giuliani, E.R., and Morse, B.S. (1974). Erythropoiesis in pyridoxine deficient mice. *Proc. Soc. Exp. Biol. Med.* **146**, 114–119.
- Kim, E., Ilagan, J.O., Liang, Y., Daubner, G.M., Lee, S.C., Ramakrishnan, A., Li, Y., Chung, Y.R., Micol, J.B., Murphy, M.E., et al. (2015). SRSF2 mutations contribute to myelodysplasia by mutant-specific effects on exon recognition. *Cancer Cell* **27**, 617–630.
- Kotake, Y., Sagane, K., Owa, T., Mimori-Kiyosue, Y., Shimizu, H., Uesugi, M., Ishihama, Y., Iwata, M., and Mizui, Y. (2007). Splicing factor SF3b as a target of the antitumor natural product pladienolide. *Nat. Chem. Biol.* **3**, 570–575.
- Kramer, A. (1996). The structure and function of proteins involved in mammalian pre-mRNA splicing. *Annu. Rev. Biochem.* **65**, 367–409.
- Kuhn, R., Schwenk, F., Aguet, M., and Rajewsky, K. (1995). Inducible gene targeting in mice. *Science* **269**, 1427–1429.
- Langemeijer, S.M., Kuiper, R.P., Berends, M., Knops, R., Aslanyan, M.G., Massouh, M., Stevens-Linders, E., van Hoogen, P., van Kessel, A.G., Raymakers, R.A., et al. (2009). Acquired mutations in TET2 are common in myelodysplastic syndromes. *Nat. Genet.* **41**, 838–842.
- Liu, J., Zhang, J., Ginzburg, Y., Li, H., Xue, F., De Franceschi, L., Chasis, J.A., Mohandas, N., and An, X. (2013). Quantitative analysis of murine terminal erythroid differentiation in vivo: novel method to study normal and disordered erythropoiesis. *Blood* **121**, e43–e49.
- Malcovati, L., Papaemmanuil, E., Bowen, D.T., Boulton, J., Della Porta, M.G., Pascutto, C., Travaglino, E., Groves, M.J., Godfrey, A.L., Ambaglio, I., et al. (2011). Clinical significance of SF3B1 mutations in myelodysplastic syndromes and myelodysplastic/myeloproliferative neoplasms. *Blood* **118**, 6239–6246.
- Matsunawa, M., Yamamoto, R., Sanada, M., Sato-Otsubo, A., Shiozawa, Y., Yoshida, K., Otsu, M., Shiraiishi, Y., Miyano, S., Isono, K., et al. (2014). Haploinsufficiency of Sf3b1 leads to compromised stem cell function but not to myelodysplasia. *Leukemia* **28**, 1844–1850.

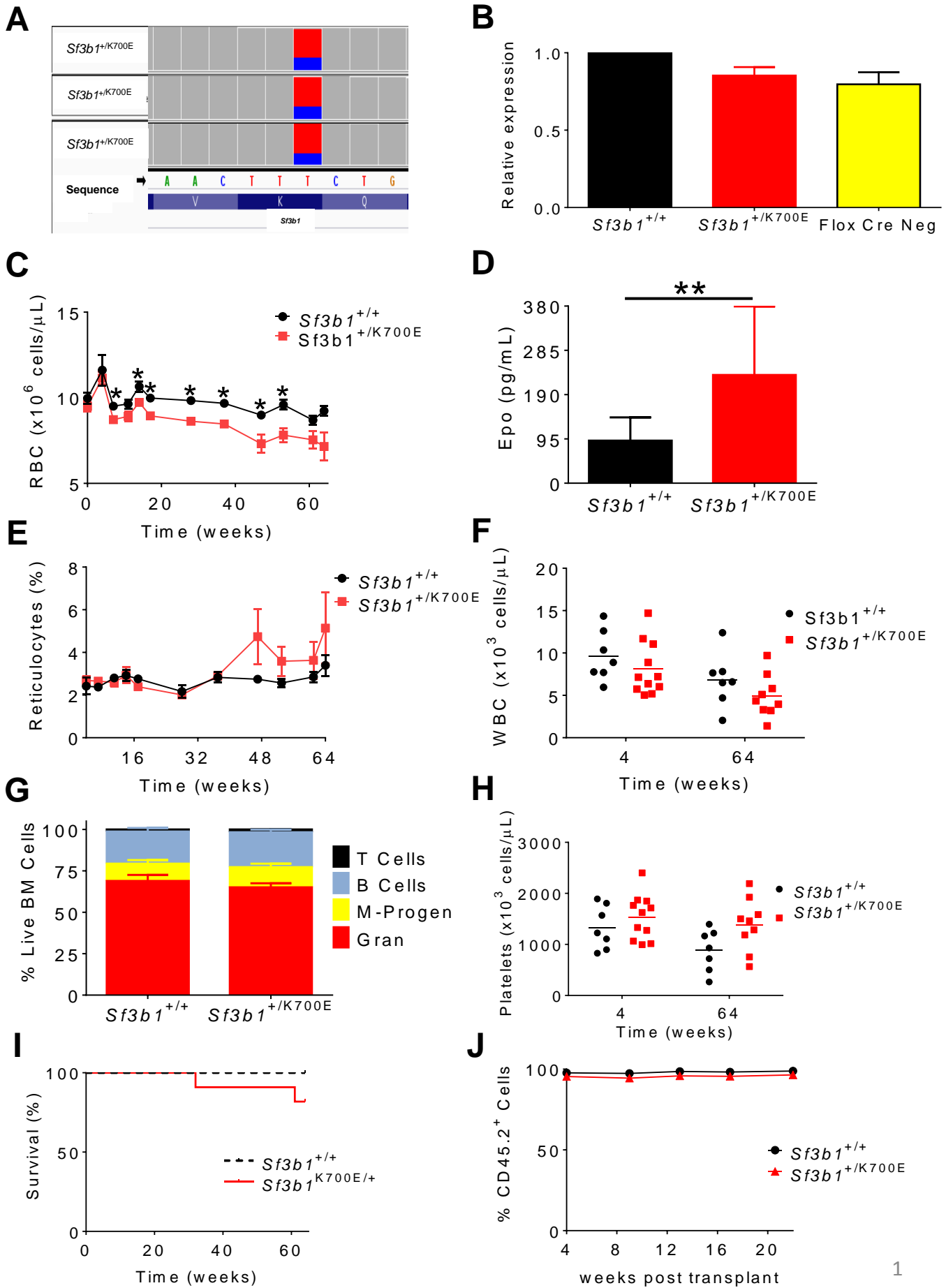
- Mizui, Y., Sakai, T., Iwata, M., Uenaka, T., Okamoto, K., Shimizu, H., Yamori, T., Yoshimatsu, K., and Asada, M. (2004). Pladienolides, new substances from culture of *Streptomyces platensis* Mer-11107. III. In vitro and in vivo anti-tumor activities. *J. Antibiot.* 57, 188–196.
- Moran-Crusio, K., Reavie, L., Shih, A., Abdel-Wahab, O., Ndiaye-Lobry, D., Lobry, C., Figueroa, M.E., Vasanthakumar, A., Patel, J., Zhao, X., et al. (2011). Tet2 loss leads to increased hematopoietic stem cell self-renewal and myeloid transformation. *Cancer Cell* 20, 11–24.
- Mufti, G.J., Bennett, J.M., Goasguen, J., Bain, B.J., Baumann, I., Brunning, R., Cazzola, M., Fenaux, P., Germing, U., Hellstrom-Lindberg, E., et al. (2008). Diagnosis and classification of myelodysplastic syndrome: International Working Group on Morphology of myelodysplastic syndrome (IWGM-MDS) consensus proposals for the definition and enumeration of myeloblasts and ring sideroblasts. *Haematologica* 93, 1712–1717.
- Nakajima, H., Hori, Y., Terano, H., Okuhara, M., Manda, T., Matsumoto, S., and Shimomura, K. (1996a). New antitumor substances, FR901463, FR901464 and FR901465. II. Activities against experimental tumors in mice and mechanism of action. *J. Antibiot.* 49, 1204–1211.
- Nakajima, H., Sato, B., Fujita, T., Takase, S., Terano, H., and Okuhara, M. (1996b). New antitumor substances, FR901463, FR901464 and FR901465. I. Taxonomy, fermentation, isolation, physico-chemical properties and biological activities. *J. Antibiot.* 49, 1196–1203.
- Papaemmanuil, E., Cazzola, M., Boultonwood, J., Malcovati, L., Vyas, P., Bowen, D., Pellagatti, A., Wainscoat, J.S., Hellstrom-Lindberg, E., Gambacorti-Passerini, C., et al. (2011). Somatic SF3B1 mutation in myelodysplasia with ring sideroblasts. *N. Engl. J. Med.* 365, 1384–1395.
- Pellagatti, A., Cazzola, M., Giagounidis, A.A., Malcovati, L., Porta, M.G., Killick, S., Campbell, L.J., Wang, L., Langford, C.F., Fidler, C., et al. (2006). Gene expression profiles of CD34+ cells in myelodysplastic syndromes: involvement of interferon-stimulated genes and correlation to FAB subtype and karyotype. *Blood* 108, 337–345.
- Pondarre, C., Campagna, D.R., Antiochos, B., Sikorski, L., Mulhern, H., and Fleming, M.D. (2007). Abcb7, the gene responsible for X-linked sideroblastic anemia with ataxia, is essential for hematopoiesis. *Blood* 109, 3567–3569.
- Quivoron, C., Couronne, L., Della Valle, V., Lopez, C.K., Plo, I., Wagner-Ballon, O., Do Cruzeiro, M., Delhommeau, F., Arnulf, B., Stern, M.H., et al. (2011). TET2 inactivation results in pleiotropic hematopoietic abnormalities in mouse and is a recurrent event during human lymphomagenesis. *Cancer Cell* 20, 25–38.
- Ren, S., Peng, Z., Mao, J.H., Yu, Y., Yin, C., Gao, X., Cui, Z., Zhang, J., Yi, K., Xu, W., et al. (2012). RNA-seq analysis of prostate cancer in the Chinese population identifies recurrent gene fusions, cancer-associated long noncoding RNAs and aberrant alternative splicings. *Cell Res.* 22, 806–821.
- Roy, S.W., and Gilbert, W. (2006). The evolution of spliceosomal introns: patterns, puzzles and progress. *Nat. Rev. Genet.* 7, 211–221.
- Shirai, C.L., Ley, J.N., White, B.S., Kim, S., Tibbitts, J., Shao, J., Ndonwi, M., Wadugu, B., Duncavage, E.J., Okeyo-Owuor, T., et al. (2015). Mutant U2AF1 expression alters hematopoiesis and Pre-mRNA splicing in vivo. *Cancer Cell* 27, 631–643.
- Socolovsky, M., Nam, H., Fleming, M.D., Haase, V.H., Brugnara, C., and Lodish, H.F. (2001). Ineffective erythropoiesis in Stat5a(-/-)5b(-/-) mice due to decreased survival of early erythroblasts. *Blood* 98, 3261–3273.
- Vardiman, J.W., Harris, N.L., and Brunning, R.D. (2002). The World Health Organization (WHO) classification of the myeloid neoplasms. *Blood* 100, 2292–2302.
- Visconte, V., Makishima, H., Jankowska, A., Szpurka, H., Traina, F., Jerez, A., O’Keefe, C., Rogers, H.J., Sekeres, M.A., Maciejewski, J.P., and Tiu, R.V. (2012a). SF3B1, a splicing factor is frequently mutated in refractory anemia with ring sideroblasts. *Leukemia* 26, 542–545.
- Visconte, V., Rogers, H.J., Singh, J., Barnard, J., Bupathi, M., Traina, F., McMahon, J., Makishima, H., Szpurka, H., Jankowska, A., et al. (2012b). SF3B1 haploinsufficiency leads to formation of ring sideroblasts in myelodysplastic syndromes. *Blood* 120, 3173–3186.
- Visconte, V., Tabarrok, A., Zhang, L., Parker, Y., Hasrouni, E., Mahfouz, R., Isono, K., Koseki, H., Sekeres, M.A., Sauntharajah, Y., et al. (2014). Splicing factor 3b subunit 1 (Sf3b1) haploinsufficient mice display features of low risk myelodysplastic syndromes with ring sideroblasts. *J. Hematol. Oncol.* 7, 89.
- Wang, L., Lawrence, M.S., Wan, Y., Stojanov, P., Sougnez, C., Stevenson, K., Werner, L., Sivachenko, A., DeLuca, D.S., Zhang, L., et al. (2011). SF3B1 and other novel cancer genes in chronic lymphocytic leukemia. *N. Engl. J. Med.* 365, 2497–2506.
- Wang, C., Sashida, G., Saraya, A., Ishiga, R., Koide, S., Oshima, M., Isono, K., Koseki, H., and Iwama, A. (2014). Depletion of Sf3b1 impairs proliferative capacity of hematopoietic stem cells but is not sufficient to induce myelodysplasia. *Blood* 123, 3336–3343.
- Welch, J.S., Ley, T.J., Link, D.C., Miller, C.A., Larson, D.E., Koboldt, D.C., Wartman, L.D., Lamprecht, T.L., Liu, F., Xia, J., et al. (2012). The origin and evolution of mutations in acute myeloid leukemia. *Cell* 150, 264–278.
- Will, C.L., and Luhrmann, R. (2011). Spliceosome structure and function. *Cold Spring Harb. Perspect. Biol.* 3, <http://dx.doi.org/10.1101/cshperspect.a003707>.
- Yoshida, K., Sanada, M., Shiraishi, Y., Nowak, D., Nagata, Y., Yamamoto, R., Sato, Y., Sato-Otsubo, A., Kon, A., Nagasaki, M., et al. (2011). Frequent pathway mutations of splicing machinery in myelodysplasia. *Nature* 478, 64–69.
- Zhang, J., Socolovsky, M., Gross, A.W., and Lodish, H.F. (2003). Role of Ras signaling in erythroid differentiation of mouse fetal liver cells: functional analysis by a flow cytometry-based novel culture system. *Blood* 102, 3938–3946.
- Zhou, Q., Derti, A., Ruddy, D., Rakiec, D., Kao, I., Lira, M., Gibaja, V., Chan, H., Yang, Y., Min, J., et al. (2015). A chemical genetics approach for the functional assessment of novel cancer genes. *Cancer Res.* 75, 1949–1958.

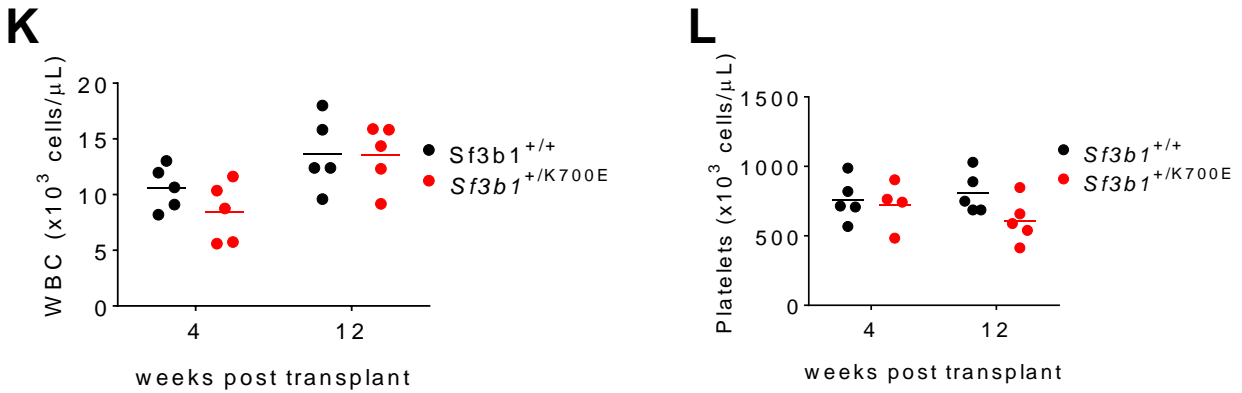
**Supplemental Information**

**Physiologic Expression of *Sf3b1*<sup>K700E</sup> Causes  
Impaired Erythropoiesis, Aberrant Splicing, and  
Sensitivity to Therapeutic Spliceosome Modulation**

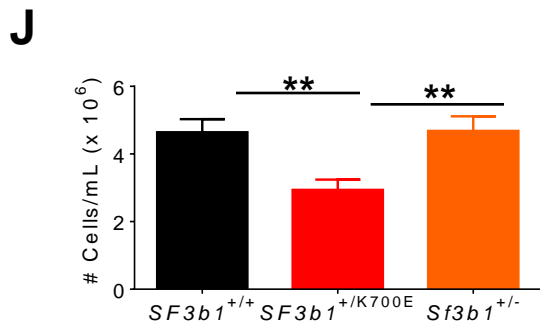
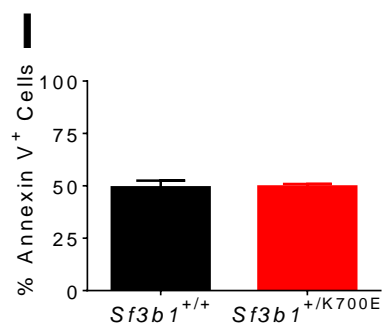
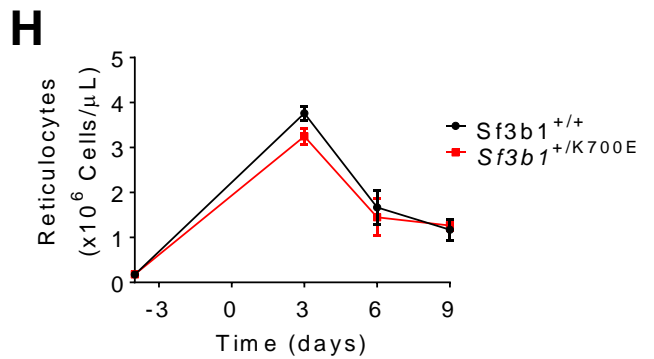
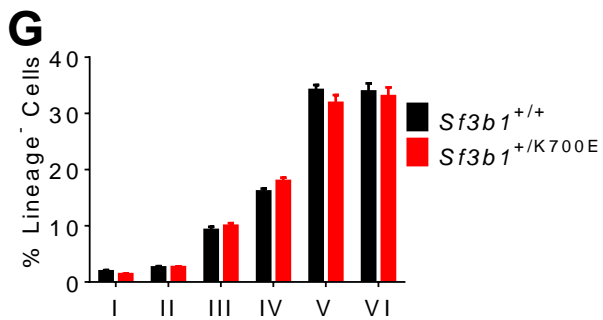
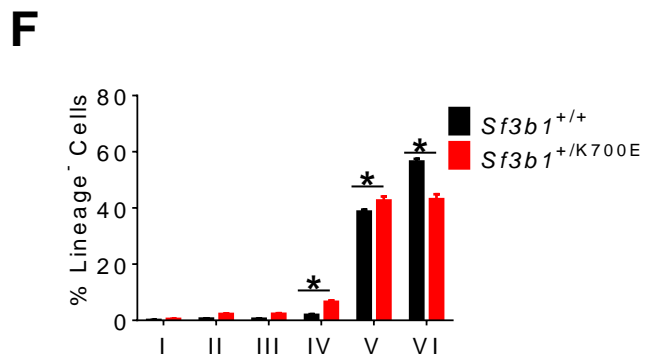
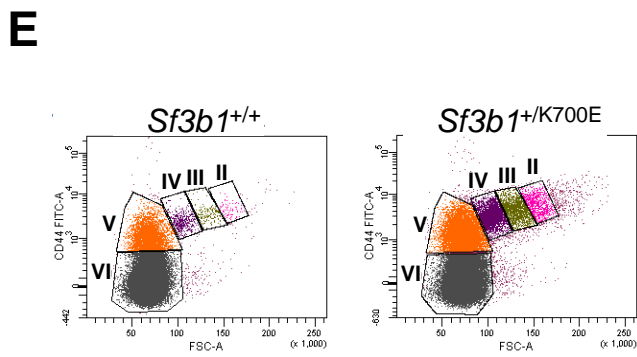
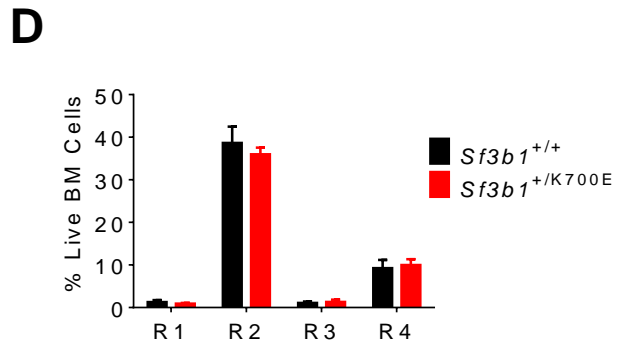
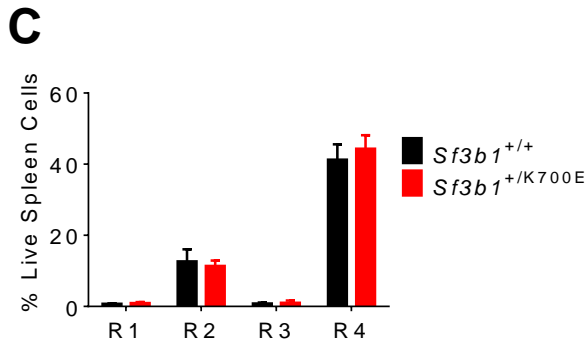
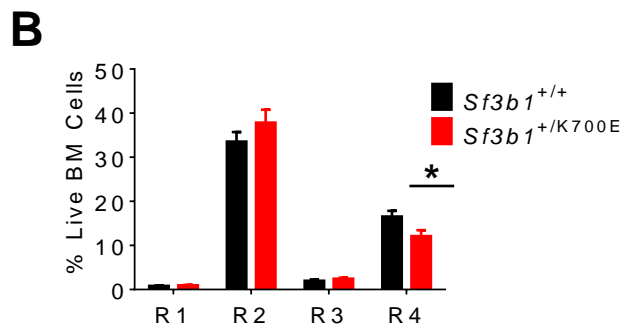
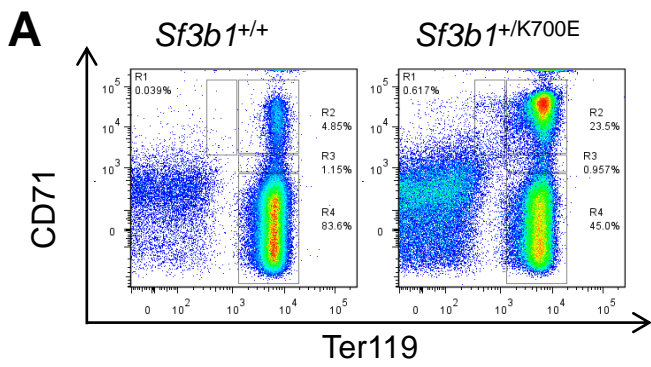
**Esther A. Obeng, Ryan J. Chappell, Michael Seiler, Michelle C. Chen, Dean R. Campagna, Paul J. Schmidt, Rebekka K. Schneider, Allegra M. Lord, Lili Wang, Rutendo G. Gambe, Marie E. McConkey, Abdullah M. Ali, Azra Raza, Lihua Yu, Silvia Buonamici, Peter G. Smith, Ann Mullally, Catherine J. Wu, Mark D. Fleming, and Benjamin L. Ebert**

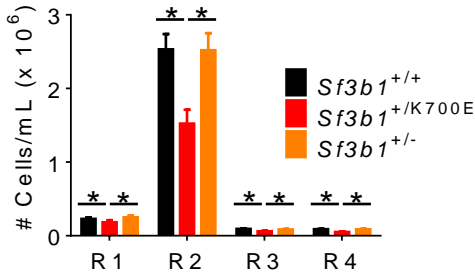
# Supplemental Data



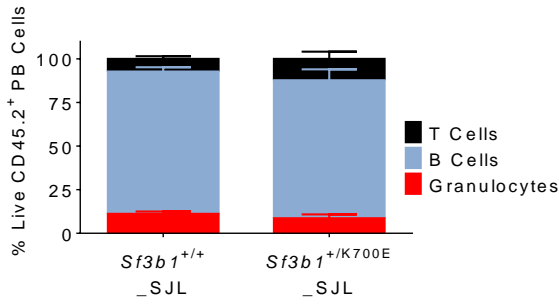
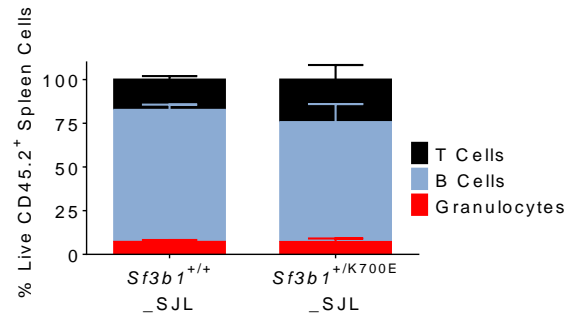
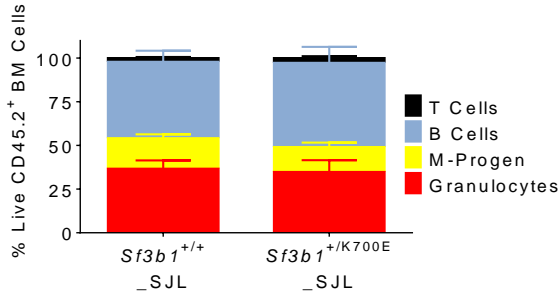


**Figure S1, related to Figure 1. Heterozygous conditional knock-in of *Sf3b1*<sup>K700E</sup> specifically results in a progressive decrease in red blood cells.** (A) Sequence fragment density from RNA sequencing performed on 3 *Sf3b1*<sup>+/K700E</sup> lineage negative, c-kit positive (LK) myeloid progenitor samples, four weeks after plpC treatment. Red denotes wild-type (adenine) and blue denotes mutant (guanine) nucleotide reads. Mutant allele frequency ranged from 27 – 32 percent. (B) Total *Sf3b1* mRNA relative to *Sf3b1*<sup>+/+</sup> mice for *Sf3b1*<sup>+/+</sup>, *Sf3b1*<sup>+/K700E</sup>, and Flox Cre negative (*Sf3b1*<sup>+/K700E</sup> *Mx1*-Cre negative) mice (n = 3 mice per group, 8 weeks post-plpC). Samples were normalized to *Gapdh*. (C) Red blood cell count over the course of 64 weeks post-plpC (n = 9 *Sf3b1*<sup>+/+</sup> and 11 *Sf3b1*<sup>+/K700E</sup> mice). (D) Plasma erythropoietin levels measured 60 weeks after plpC induction (n = 14 *Sf3b1*<sup>+/+</sup> and 16 *Sf3b1*<sup>+/K700E</sup> mice). (E) Reticulocyte percentage over the course of 64 weeks post-plpC (n = 9 *Sf3b1*<sup>+/+</sup> and 11 *Sf3b1*<sup>+/K700E</sup> mice). (F) White blood cell counts 4 weeks and 64 weeks after plpC induction (n = 9 *Sf3b1*<sup>+/+</sup> and 11 *Sf3b1*<sup>+/K700E</sup> mice). (G) Percentage of mature white blood cells in the bone marrow of 9 *Sf3b1*<sup>+/+</sup> and 11 *Sf3b1*<sup>+/K700E</sup> mice, 64 weeks post-plpC. Gran: Granulocytes: Gr1<sup>hi</sup> CD11b<sup>+</sup>. M-progen: Myeloid progenitors (Gr1<sup>lo</sup> CD11b<sup>+</sup>), B cells B220<sup>+</sup>, T cells CD3<sup>+</sup>. (H) Platelet counts for *Sf3b1*<sup>+/+</sup> and *Sf3b1*<sup>+/K700E</sup> mice, 4 weeks and 64 weeks after plpC induction (n = 9 *Sf3b1*<sup>+/+</sup> and 11 *Sf3b1*<sup>+/K700E</sup> mice). (I) Kaplan-Meier survival curve for *Sf3b1*<sup>+/K700E</sup> mice and *Sf3b1*<sup>+/+</sup> littermate controls (n = 9 *Sf3b1*<sup>+/+</sup> and 11 *Sf3b1*<sup>+/K700E</sup> mice). (J) Percentage of CD45.2 donor chimerism in the peripheral blood over the course of 20 weeks after noncompetitive transplantation assay. One million unfractionated bone marrow cells from CD45.2<sup>+</sup> *Sf3b1*<sup>+/+</sup> or *Sf3b1*<sup>+/K700E</sup> mice were transplanted into lethally irradiated (10.5 Gy) CD45.1<sup>+</sup> B6.SJL recipients (n = 5 mice per group). (K - L) White blood cell (K) and platelet (L) counts for *Sf3b1*<sup>+/+</sup> and *Sf3b1*<sup>+/K700E</sup> recipients, 4 weeks and 12 weeks after noncompetitive transplantation (n = 5 mice per group; horizontal lines indicate the mean). Data presented as mean  $\pm$  SEM. \* p < 0.05; \*\* p < 0.001. Horizontal line indicates the mean for the scatter dot plots.

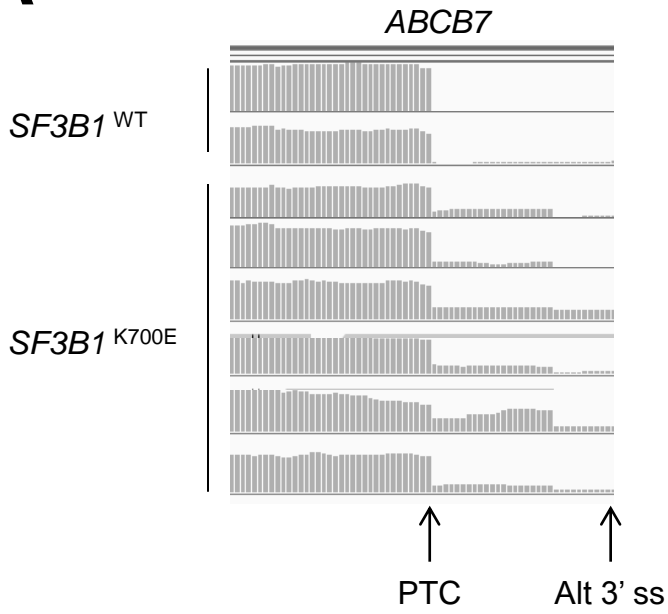
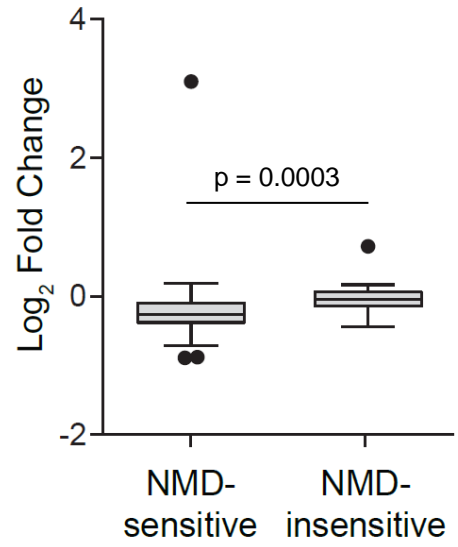
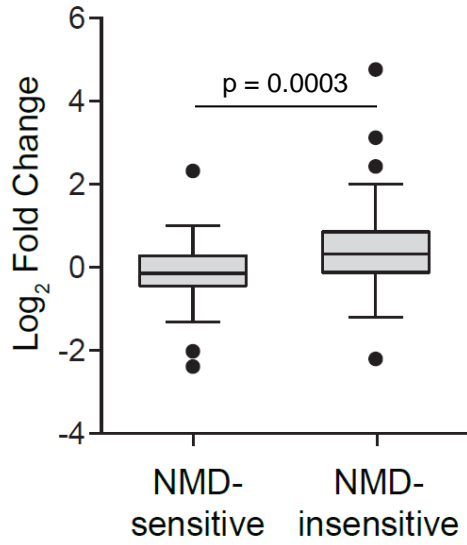


**K**

**Figure S2, related to Figure 2. *Sf3b1*<sup>K700E</sup> causes a block in terminal erythroid maturation.** (A) Representative flow cytometry plot for CD71 (transferrin receptor) and Ter119 staining of erythroid precursors from the spleen of a *Sf3b1*<sup>+/+</sup> and a *Sf3b1*<sup>+/K700E</sup> mouse, as indicated. (B) Analysis of terminal erythroid maturation in the bone marrow of *Sf3b1*<sup>+/+</sup> and *Sf3b1*<sup>+/K700E</sup> mice, 64 weeks after plpC treatment (n = 9 *Sf3b1*<sup>+/+</sup> and 11 *Sf3b1*<sup>+/K700E</sup> mice). (C - D) Analysis of terminal erythroid maturation in the spleens (C) and bone marrow (D) of *Sf3b1*<sup>+/+</sup> and *Sf3b1*<sup>+/K700E</sup> mice, 12 weeks post plpC treatment (n = 5 *Sf3b1*<sup>+/+</sup> and 6 *Sf3b1*<sup>+/K700E</sup> mice). (E) Representative flow cytometry plot using CD44 staining and forward scatter to characterize erythroid maturation in *Sf3b1*<sup>+/+</sup> and *Sf3b1*<sup>+/K700E</sup> mice. Erythroid maturation can be quantified from the stage II basophilic erythroblast to the stage VI mature red blood cell, as indicated. (F - G) Percentage cells in each stage of terminal erythroid maturation in the spleen (F) and bone marrow (G) of *Sf3b1*<sup>+/+</sup> and *Sf3b1*<sup>+/K700E</sup> mice, 52 weeks post plpC treatment (n = 6 *Sf3b1*<sup>+/+</sup> and 7 *Sf3b1*<sup>+/K700E</sup> mice). (H) Absolute reticulocyte count [(% reticulocytes/100) x red blood cell count] measured 4 days before and 3, 6, and 9 days after the first injection of *Sf3b1*<sup>+/+</sup> and *Sf3b1*<sup>+/K700E</sup> animals with phenylhydrazine (PHZ; n = 11 *Sf3b1*<sup>+/+</sup> and 10 *Sf3b1*<sup>+/K700E</sup> mice). (I) Percentage of Annexin V positive cells 48 hr after c-kit<sup>+</sup> progenitor cells were plated in erythroid differentiation medium. Triplicate samples were run on 3 mice per group. (J) Absolute number of *Sf3b1*<sup>+/+</sup>, *Sf3b1*<sup>+/K700E</sup>, or *Sf3b1*<sup>+/-</sup> cells in culture 48 hr after 2.0 x 10<sup>5</sup> bone marrow c-Kit<sup>+</sup> progenitor cells were plated in erythroid differentiation medium. Triplicate samples were analyzed from each of 3 mice per group. (K) Analysis of the total number of cells in each stage of terminal erythroid maturation 48 hr after bone marrow c-Kit<sup>+</sup> progenitor cells from *Sf3b1*<sup>+/+</sup>, *Sf3b1*<sup>+/K700E</sup>, or *Sf3b1*<sup>+/-</sup> mice were plated in erythroid differentiation medium. Triplicate samples were analyzed from each of 3 mice per group. Data presented as mean ± SEM. \* p < 0.05; \*\* p < 0.01.

**A****B****C**

**Figure S3, related to Figure 3. Heterozygous conditional knock-in of *Sf3b1*<sup>K700E</sup> does not alter the distribution of mature white blood cell lineages in competitive transplantation recipients.** (A - C) Percentage of mature white blood cells in the peripheral blood (A), spleen (B) and bone marrow (C) of recipient mice, 20 weeks after competitive repopulation assay. One million unfractionated bone marrow cells from CD45.2<sup>+</sup> *Sf3b1*<sup>+/+</sup> or *Sf3b1*<sup>+/K700E</sup> mice were mixed 1:1 with 1 x 10<sup>6</sup> CD45.1<sup>+</sup> B6.SJL unfractionated bone marrow cells and transplanted into lethally irradiated (10.5 Gy) B6.SJL recipients (n = 5 mice per group). Granulocytes: Gr1<sup>hi</sup> CD11b<sup>+</sup>. M-progen: Myeloid progenitors (Gr1<sup>lo</sup> CD11b<sup>+</sup>), B cells B220<sup>+</sup>, T cells CD3<sup>+</sup>. Data presented as mean ± SEM. \* p < 0.05.

**A****B****C**

**Figure S4, related to Figure 4. Over 30% of all aberrantly spliced genes in SF3B1-mutant cells are putative targets of nonsense mediated decay (NMD). (A)**

Sequence fragment density from RNA sequencing performed on two *SF3B1* wild-type and six *SF3B1*-mutant MDS patient samples. An aberrant 3' splice site between exon 8 and exon 9 of *ABCB7* caused the addition of a premature termination codon (PTC) within a seven amino acid addition to the protein sequence, prior to the start of the next canonical exon as described previously for *SF3B1*-mutant isogenic Nalm-6 cells. (B) Comparison of whole gene expression of predicted NMD sensitive (n = 22) and NMD insensitive (n = 36) transcripts given as the log<sub>2</sub> fold change between *Sf3b1*<sup>+/K700E</sup> and *Sf3b1*<sup>+/+</sup> myeloid progenitors (LK cells, n = 3 mice per group). NMD predictions were derived from aberrant junctions identified in *Sf3b1*<sup>+/K700E</sup> myeloid progenitor samples (see Table S1). Box plots and whiskers are represented as per the Tukey method. (C) Comparison of whole gene expression of predicted NMD sensitive (n = 36) and NMD insensitive (n = 72) transcripts given as the log<sub>2</sub> fold change between *SF3B1*-mutant and *SF3B1* wild-type MDS patient samples. NMD predictions were derived from aberrant junctions identified in *SF3B1*-mutant patient samples (see Table S2). Data presented as mean ± SEM.

**Table S1, related to Figure 4. List of Aberrant Splice Junctions and Predicted NMD Candidates Identified in Sf3b1K700E Myeloid Progenitor Cells. Provided as an Excel File.**

**Table S2, related to Figure 4. List of Aberrant Splice Junctions and Predicted NMD Candidates Identified in SF3B1-Mutant MDS Patient Sample Bone Marrow. Provided as an Excel File.**

**Table S3, related to Figure 4. Significantly Upregulated and Downregulated Pathways Identified by GSEA**

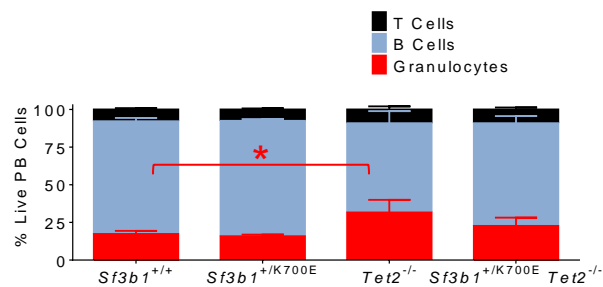
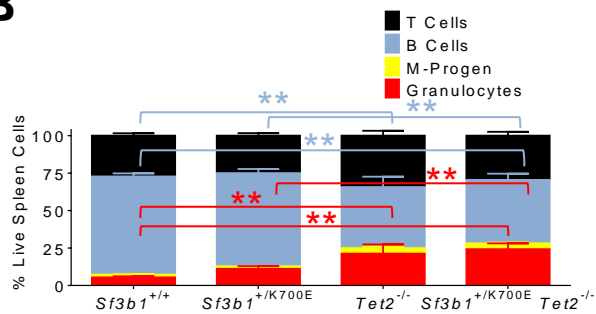
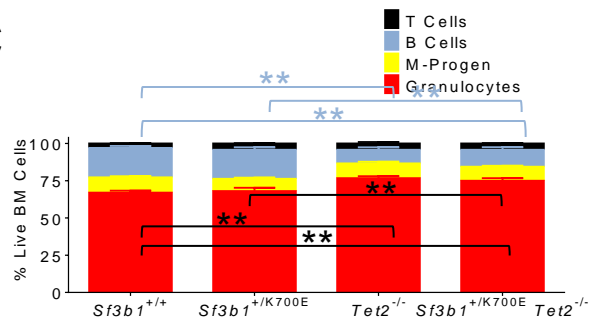
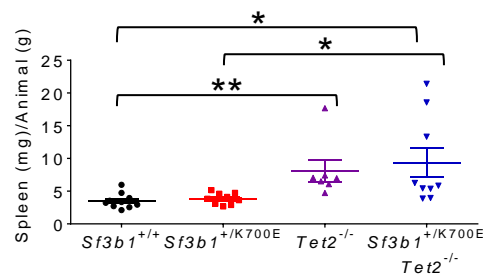
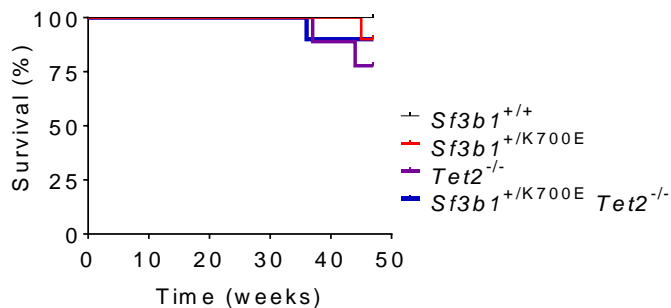
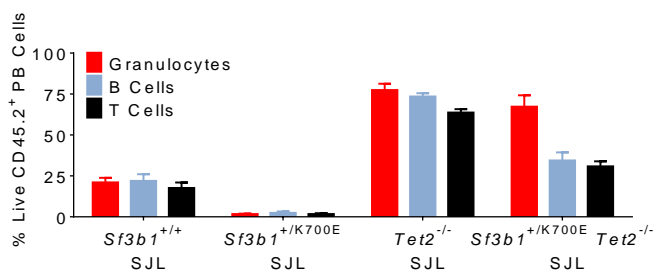
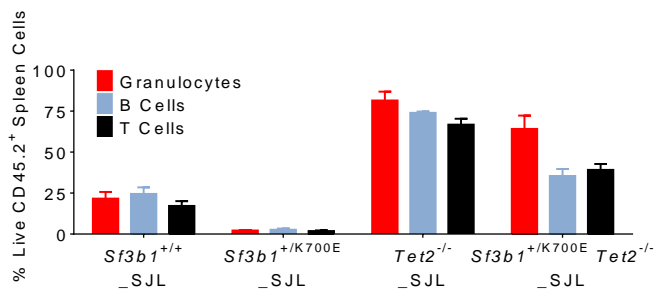
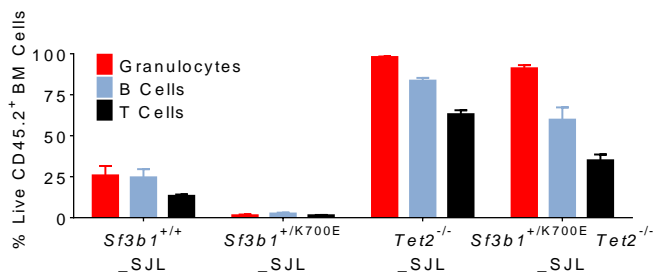
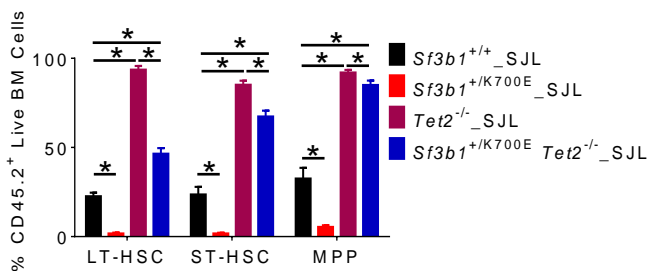
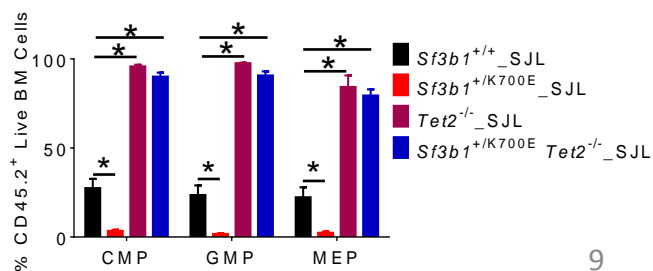
<b><u>MDS UP</u></b>	<b><u>LK UP</u></b>
Ribosome Peptide Chain Elongation	<b>RPS14 Down V1 Up</b>
3' UTR <sup>1</sup> Mediated Translational Regulation	
Ribosome	
Translation	
Nonsense Mediated Decay Enhanced by the Exon Junction Complex	
Structural Constituent of Ribosome	
Metabolism of mRNA	
Metabolism of Proteins	
Translated RNA	
Peptide Chain Elongation	
RNA Binding	
<b>RPS14<sup>2</sup> Down V1 Up</b>	
<b><u>MDS DOWN</u></b>	<b><u>LK DOWN</u></b>
<b>Heme Metabolism</b>	Ribosome
Cell Cycle	RNA Binding
<b>Cell Cycle Mitotic</b>	3' UTR Mediated Translational Regulation
DNA Replication	Metabolism of RNA
Normal Quiescent vs Normal Dividing Down	Metabolism of mRNA
CML Dividing vs Normal Quiescent Up	Translation
Hematopoiesis Mature Cell	Transcription
Proliferation	<b>Cell Cycle Mitotic</b>
CDC27 <sup>3</sup>	RNA Splicing
RRM1 <sup>4</sup>	mRNA Processing
Cell Cycle G0	
Response to DNA Damage Stimulus	<b>RPS14 Down V1 Down</b>
Regulation of Cell Cycle	<b>G2-M Checkpoint</b>
<b>RPS14 Down V1 Down</b>	<b>Heme Metabolism</b>
<b>G2-M Checkpoint</b>	

<sup>1</sup>Untranslated Region

<sup>2</sup>Ribosomal Protein S14

<sup>3</sup>Cell Division Cycle 27

<sup>4</sup>Ribonucleotide Reductase M1

**A****B****C****D****E****F****G****H****I****J**

**Figure S5, related to Figure 5. *Sf3b1*<sup>+/*K700E*</sup> *Tet2*<sup>-/-</sup> double mutant mice have additional features of MDS and a competitive advantage in repopulation experiments.** (A - C) Percentage of mature white blood cells in the peripheral blood (A), spleen (B) and bone marrow (C) of *Sf3b1*<sup>+/+</sup>, *Sf3b1*<sup>+/*K700E*</sup>, *Tet2*<sup>-/-</sup> and *Sf3b1*<sup>+/*K700E*</sup> *Tet2*<sup>-/-</sup> primary mice, 45 weeks post-plpC (n = 7 - 10 mice per group). Granulocytes: Gr1<sup>hi</sup> CD11b<sup>+</sup>. M-progen: Myeloid progenitors (Gr1<sup>lo</sup> CD11b<sup>+</sup>), B cells B220<sup>+</sup>, T cells CD3<sup>+</sup>. (D) Normalized spleen weights [spleen weight (mg) / animal weight (g)] from *Sf3b1*<sup>+/+</sup>, *Sf3b1*<sup>+/*K700E*</sup>, *Tet2*<sup>-/-</sup> and *Sf3b1*<sup>+/*K700E*</sup> *Tet2*<sup>-/-</sup> primary mice, 45 weeks post-plpC (n = 7 - 10 mice per group). (E) Kaplan-Meier survival curve for the group of *Sf3b1*<sup>+/+</sup>, *Sf3b1*<sup>+/*K700E*</sup>, *Tet2*<sup>-/-</sup> and *Sf3b1*<sup>+/*K700E*</sup> *Tet2*<sup>-/-</sup> primary mice (n = 9 - 10 mice per group). (F - H) Percentage of mature white blood cells in the peripheral blood (F), spleen (G) and bone marrow (H) of recipient mice, 20 weeks after competitive repopulation assay. One million unfractionated bone marrow cells from CD45.2<sup>+</sup> *Sf3b1*<sup>+/+</sup>, *Sf3b1*<sup>+/*K700E*</sup>, *Tet2*<sup>-/-</sup> or *Sf3b1*<sup>+/*K700E*</sup> *Tet2*<sup>-/-</sup> mice were mixed 1:1 with 1 x 10<sup>6</sup> CD45.1<sup>+</sup> B6.SJL unfractionated bone marrow cells and transplanted into lethally irradiated (10.5 Gy) B6.SJL recipients (n = 5 mice per group). Granulocytes: Gr1<sup>hi</sup> CD11b<sup>+</sup>, B cells B220<sup>+</sup>, T cells CD3<sup>+</sup>. (I) Analysis of the percentage of LT-HSCs, ST-HSCs, and MPPs in the bone marrow of *Sf3b1*<sup>+/+</sup>, *Sf3b1*<sup>+/*K700E*</sup>, *Tet2*<sup>-/-</sup>, and *Sf3b1*<sup>+/*K700E*</sup> *Tet2*<sup>-/-</sup> mice, 24 weeks after competitive repopulation assay (n = 5 mice per group). (J) Analysis of the percentage of CMPs, GMPs, and MEPs in the bone marrow of *Sf3b1*<sup>+/+</sup>, *Sf3b1*<sup>+/*K700E*</sup>, *Tet2*<sup>-/-</sup>, and *Sf3b1*<sup>+/*K700E*</sup> *Tet2*<sup>-/-</sup> mice, 24 weeks after competitive repopulation assay (n = 5 mice per group). Data presented as mean ± SEM. \* p < 0.05; \*\* p < 0.01.

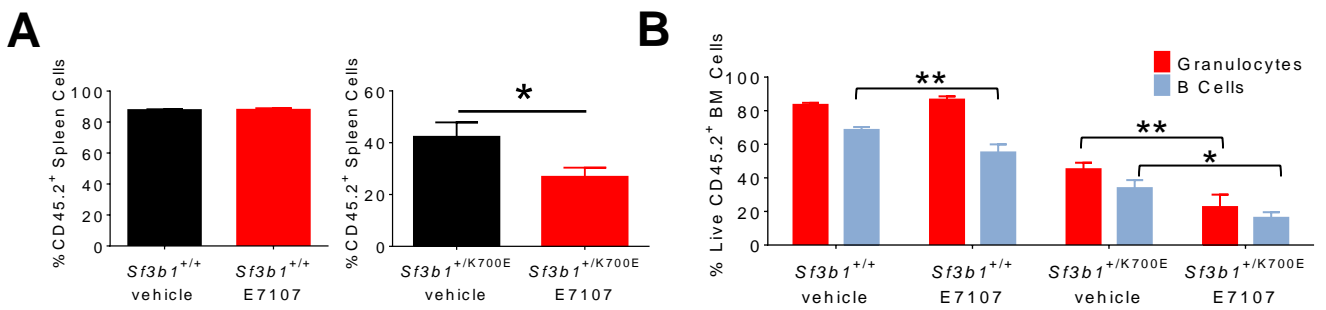


**Figure S6, related to Figure 6. *Sf3b1*<sup>K700E</sup> expressing cells are sensitive to the spliceosome modulator, E7107, in vivo.** (A) Percentage of CD45.2<sup>+</sup> donor chimerism in the spleen of *Sf3b1*<sup>+/+</sup> or *Sf3b1*<sup>+/*K700E*</sup> recipients treated with E7107 or vehicle (n = 5 mice per group). (B) Mature myeloid and lymphoid cell chimerism in the bone marrow of *Sf3b1*<sup>+/+</sup> and *Sf3b1*<sup>+/*K700E*</sup> competitive transplant recipients treated with E7107 or vehicle (n = 5 mice per group). Granulocytes: Gr1<sup>+</sup>. B cells B220<sup>+</sup>. Data presented as mean ± SEM. \* p < 0.05; \*\* p < 0.01.

## Supplemental Experimental Procedures

### Generation of a *Sf3b1*<sup>K700E</sup> Conditional Knock-In Mouse

Mouse embryonic stem cells with a targeting construct containing inverted copies of exons 15 (with the K700E mutation) and 16 in a C57BL/6/129 genetic background were generated by Biocytogen (Worcester, MA). The neomycin/*lacZ* cassette was flipped out *in vitro* by transfection of a plasmid expressing the flippase recombinase (FRT).

Successful FRT recombination was validated by PCR (forward primer: 5'-TCGCACTTGAGC TATTGGGGAGT-3'; reverse primer: 5'-AGGCATGGTAGCTCACACCTGA-3'). Following confirmation of germline transmission, mice were crossed with the Mx1-Cre mouse strain (Jackson Laboratory, stock number 002527). To cause inversion of exons 15 and 16, *Sf3b1*<sup>fl/+</sup> mice were given four rounds of poly(I:C) (InvivoGen, San Diego, CA) by intraperitoneal injection. *Sf3b1*<sup>+/K700E</sup> mice were backcrossed against C57BL/6J inbred mice for 9 generations. Littermate controls were used for all experiments, unless stated otherwise in the figure legends.

### Antibodies and Reagents

Bone marrow cells were isolated by flushing and crushing pelvic and hind leg bones with PBS (Life Technologies™) + 2% fetal bovine serum (FBS) + penicillin/streptomycin (Life Technologies™). Whole bone marrow was lysed on ice with red blood cell lysis solution (Invitrogen/ Life Technologies™), and washed in PBS (Life Technologies™) plus 2% FBS. Single-cell suspensions of spleen were prepared by pressing tissue through a 70 μM cell strainer followed by red blood cell lysis. Cells were labeled with monoclonal antibodies in 2% FBS/PBS for 30 min on ice and analyzed using an LSR II flow cytometer (BD Biosciences). Antibodies and reagents are listed in the table below:

Antibodies/Reagents Used for Flow Cytometry						
	Fluorochrome	Company	Fluorochrome	Company	Fluorochrome	Company
live/dead	Dapi	Roche Diagnostics				
Gr1	efluor 450	eBioscience	APCCy7	eBioscience	APC	eBioscience
B220	efluor 450	eBioscience	APCCy7	eBioscience	PECy7	BD Pharmingen
CD3	efluor 450	eBioscience	APCCy7	eBioscience		
CD11b	efluor 450	eBioscience	APCCy7	eBioscience		
Ter119	efluor 450	eBioscience	APCCy7	eBioscience	APC	eBioscience
CD150	PE/Cy5	Biolegend				
CD48	APCCy7	Biolegend				
CD34	FITC	eBioscience				
CD16/32	PE	eBioscience				
Sca1	PECy7	eBioscience				
c-kit	APC	eBioscience				
CD45.1	PE	eBioscience				
CD45.2	FITC	eBioscience				
Annexin V	APC	BD Pharmingen				
CD71	PE	eBioscience				
CD44	FITC	BD Biosciences				
CD45	APCCy7	BD Pharmingen				
Ki67	FITC	BD Pharmingen				
Hoechst		Life Technologies				

### **Erythropoietin Assay**

100 mL serum was used in Mouse Erythropoietin Quantikine ELISA Kit (R&D Systems, Minneapolis, MN) according to the manufacturer's instructions.

### **Phenylhydrazine Stress Test**

PHZ (Sigma-Aldrich) was diluted in PBS and 30 mg/kg was injected subcutaneously on 2 consecutive days (day 0 and day +1). Blood was collected 4 days prior to injection and at days 3, 6, and 9-post injection for hemoglobin and reticulocyte count measurements.

### **Colony-Forming Assays**

Whole BM and spleen cells were harvested, subjected to RBC lysis, and resuspended in IMDM with 10% FBS and 5% penicillin-streptomycin. Cells were plated in triplicate in M3434 methylcellulose media (Stem Cell Technologies) at 20,000 cells/dish. Colonies were scored after 7 days.

### **Histopathology**

Murine organs were fixed in formalin with 3.7% paraformaldehyde, and histology slides were prepared and stained by the Brigham and Women's core Rodent Histology Facility. Digital images were acquired using a Nikon Eclipse E400 microscope equipped with a digital camera and analyzed using Spot Advanced software (model 2.1.1, Diagnostic Instruments).

### **Repopulation and Transplantation Assays**

For competitive repopulation experiments, competitor bone marrow was obtained from age-matched B6.SJL mice. Transplant recipients were 6- to 8-week-old B6.SJL mice. For lethal irradiation, mice were given 1 doses of 10.5 cGy on the day prior to transplant. Donor bone marrow was injected into the retro-orbital plexus.

### **Primary Murine Cell Isolation and Culture**

c-kit<sup>+</sup> cells were isolated from whole bone marrow using the autoMACS pro Separator (Miltenyi Biotec). C-kit<sup>+</sup> bone marrow cells cultured in StemSpan™ Serum-Free Expansion Medium (Stem Cell Technologies) supplemented with murine thrombopoietin (m-tpo) (50 ng/mL; Peprtech), and murine stem cell factor (m-scf) (50 ng/mL; Peprtech).

### **Quantitative Real-Time PCR (qRT-PCR)**

Unfractionated bone marrow cells were isolated as described above from *Sf3b1*<sup>+/+</sup>, *Sf3b1*<sup>+/*K700E*</sup>, and Flox Cre negative (*Sf3b1*<sup>+/*K700E*</sup> *Mx1*-Cre negative) mice. The bone marrow cells were lysed with TRIzol® Reagent (Invitrogen / Life Technologies), according to the manufacturer's specifications for RNA extraction. Purified RNA was dissolved in sterile distilled water. cDNA was synthesized using the QuantiTect Reverse Transcription Kit (Qiagen), according to the manufacturer's protocol. qRT-PCR reactions were performed using TaqMan Expression Assays for *Sf3b1* and *Gapdh* genes (Applied Biosystems) and TaqMan Universal PCR Mastermix (Applied Biosystems) in an ABI Prism 7900 Real-Time PCR System (Applied Biosystems). Each condition was run in triplicate. Expression of *Sf3b1* was normalized to *Gapdh*.

### **Quantification of RNA sequencing data**

RNA sequencing analysis was performed as described previously (Darman et al., 2015). Briefly, for all RNA-seq data, reads were aligned to hg19 by STAR (Dobin et al., 2013), gene isoform counts were quantified by Sailfish (Li and Dewey, 2011) against

GENCODE annotation version v19. Gene and isoform quantification is given in unit of TPM (transcripts per million). Raw junction counts generated by STAR were used for all further downstream analyses; however splice junctions which did not meet a minimum average threshold of 10 counts in either wild-type SF3B1 or SF3B1-mutant cohorts were removed in order to reduce false positives. In order to identify intron retention events, estimates of read counts spanning each intron-exon junction were required. For every splice junction in each BAM file, we counted reads which fully overlapped artificially defined 6 bp regions, 3 bp intronic and 3 bp exonic, across each of the 3' and 5' intron-exon junctions.

### **Identification of Differential Splice Junctions**

Analysis was performed as described previously (Darman et al., 2015). Briefly, instead of raw splice junction counts obtained during the quantification process, percentages of splice junctions relative to shared splice sites were calculated and used to assess differential splicing activities between SF3B1-mutant and wild-type SF3B1. In brief, the junction usage percentage, or percent spliced in (PSI) is a measurement of the usage of one splice junction relative to all other splice junctions that share the same splice site. Therefore for each shared splice site, the raw counts of each splice junction are divided by the total counts of all splice junctions that utilize the same shared splice site in order to derive a ratio which is then multiplied by 100 to convert to a percentage. Differential PSI was assessed between SF3B1-mutant and wild-type SF3B1 using moderated t-test defined in the Bioconductor's limma package (Wettenhall and Smyth, 2004). The statistical p values were corrected using the Benjamini-Hochberg procedure.

Canonical splice junctions were identified as those junctions which shared a splice site with an aberrant junction and which were also differentially upregulated in the wild-type SF3B1 setting, i.e., exhibit "switch-like" behavior. To be conservative, we reported only those aberrant junctions which had corresponding canonical splice junctions which could also pass a q-value threshold of 0.20. Intron retention events were required to be upregulated (have significantly differential PSI between SF3B1-mutant and wild-type SF3B1) for both 3' and 5' intron-exon junctions as defined above. The canonical junction was therefore defined to be the junction which spans the intronic sequence, and this was also required to be upregulated in wild-type SF3B1 as was required for all other canonical splicing events.

### **Motif and Cross-Species Analyses**

Analysis was performed as described previously (Darman et al., 2015). Briefly, consensus sequences for 3' splice sites were defined using 35 intronic bases upstream and 3 exonic bases downstream of both aberrant AGs preferentially used by SF3B1-mutant and canonical AGs preferentially used by wild-type SF3B1. All alternative 3' splice motifs were derived from cryptic AGs found upstream of their canonical 3' splice sites. Reference 3' splice sites were derived from hg19 (human) and mm10 (mouse) annotations given in RefSeq (Tatusova et al., 2014), KnownGene (Hsu et al., 2006), AceView (Thierry-Mieg and Thierry-Mieg, 2006), and Ensembl (Cunningham et al., 2015) databases. Pictograms of consensus sequences were generated using WebLogo (Crooks et al., 2004). In cases where the number of sequences exceeded 2000 (as in all reference 3' splice sites), 2000 sequences were randomly sampled in order to generate the image.

### **NMD Prediction**

Analysis was performed as described previously (Darman et al., 2015). Briefly, the existence of PTCs found > 55 nt upstream from the last exon-exon junction in a

transcript has been shown to be most predictive of degradation by NMD (Rivas et al., 2015). In order to predict the location of PTCs in transcripts, we attempted to predict the complete sequence of all RefSeq transcripts which could contain the aberrant junction, e.g., an alternative 3' ss shares its 5' ss with a known RefSeq transcript, causing the elongation of the downstream exon. If a given transcript contained more than one aberrant junction, changes effected by each aberrant junction were applied and evaluated independently. Additionally, we detect aberrant transcripts which extend well beyond the canonical transcript termination (lack of PTC), which have been shown to be subject to nonstop mediated decay, a separate pathway which nonetheless results in transcript degradation (Wu and Brewer, 2012). Protein sequence prediction was carried out for each transcript independently using standard codon translation of the coding sequence. Each prediction is given as either a) True, a PTC is predicted > 55 nt from the final exon-exon junction in all RefSeq transcripts which could contain the aberrant junction, b) False, no PTCs < 55 nt upstream from the last exon-exon junction would be generated in any RefSeq transcript, c) Ambiguous, some transcripts which could contain the aberrant transcript at that gene locus are predicted to be NMD targets while others are not, and d) No CDS, which is assigned if the aberrant junction does not affect genes with any coding transcripts (lncRNA, etc) or the aberrant junction could not be assigned to any known RefSeq transcript.

### **Gene Set Enrichment Analysis (GSEA)**

To identify pathways that were enriched in the sorted Sf3b1<sup>+ /K700E</sup> myeloid progenitor (LK, n = 3) and SF3B1-mutant MDS patient bone marrow mononuclear cells (n = 6), Gene Set Enrichment Analysis (GSEA; <http://www.broadinstitute.org/gsea/msigdb/annotate.jsp>) was performed on genes which were consistently upregulated or downregulated in Sf3b1<sup>+ /K700E</sup> myeloid progenitor (LK) or SF3B1-mutant unfractionated bone marrow samples when compared to wild-type controls (n = 3 Sf3b1<sup>+/+</sup> and n = 4 wild-type SF3B1 MDS patient samples).

## Supplemental References

Crooks, G. E., Hon, G., Chandonia, J. M., and Brenner, S. E. (2004). WebLogo: a sequence logo generator. *Genome research* 14, 1188-1190.

Cunningham, F., Amode, M. R., Barrell, D., Beal, K., Billis, K., Brent, S., Carvalho-Silva, D., Clapham, P., Coates, G., Fitzgerald, S., *et al.* (2015). Ensembl 2015. *Nucleic acids research* 43, D662-669.

Dobin, A., Davis, C. A., Schlesinger, F., Drenkow, J., Zaleski, C., Jha, S., Batut, P., Chaisson, M., and Gingeras, T. R. (2013). STAR: ultrafast universal RNA-seq aligner. *Bioinformatics* 29, 15-21.

Hsu, F., Kent, W. J., Clawson, H., Kuhn, R. M., Diekhans, M., and Haussler, D. (2006). The UCSC Known Genes. *Bioinformatics* 22, 1036-1046.

Li, B., and Dewey, C. N. (2011). RSEM: accurate transcript quantification from RNA-Seq data with or without a reference genome. *BMC bioinformatics* 12, 323.

Rivas, M. A., Pirinen, M., Conrad, D. F., Lek, M., Tsang, E. K., Karczewski, K. J., Maller, J. B., Kukurba, K. R., DeLuca, D. S., Fromer, M., *et al.* (2015). Human genomics. Effect of predicted protein-truncating genetic variants on the human transcriptome. *Science* 348, 666-669.

Tatusova, T., Ciufu, S., Fedorov, B., O'Neill, K., and Tolstoy, I. (2014). RefSeq microbial genomes database: new representation and annotation strategy. *Nucleic acids research* 42, D553-559.

Thierry-Mieg, D., and Thierry-Mieg, J. (2006). AceView: a comprehensive cDNA-supported gene and transcripts annotation. *Genome biology* 7 *Suppl 1*, S12 11-14.

Wettenhall, J. M., and Smyth, G. K. (2004). limmaGUI: a graphical user interface for linear modeling of microarray data. *Bioinformatics* 20, 3705-3706.

Wu, X., and Brewer, G. (2012). The regulation of mRNA stability in mammalian cells: 2.0. *Gene* 500, 10-21.